Electronic Processes at Organic−Organic Interfaces: Insight from Modeling and Implications for Opto-electronic Devices[†]

David Beljonne,*[,‡,§] Jérôme Cornil,[‡,§] Luca Muccioli,[⊥] Claudio Zannoni,[⊥]
Jean-Luc Brédas,[§,‡] and Frédéric Castet[#]

[‡]*Laboratory for Chemistry of Novel Materials, University of Mons, Place du Parc 20, B-7000 Mons,
Belgium,* [§]*School of Chemistry and Biochemistry and Center for Organic Photonics and Electronics, Georgia
Institute of Technology, Atlanta, Georgia 30332-0400, United States,* [⊥]*Dipartimento di Chimica Fisica e
Inorganica and INSTM, Università di Bologna, IT-40136 Bologna, Italy, and* [#]*Institut des Sciences
Moléculaires, UMR CNRS 5255, Université de Bordeaux, Cours de la Libération 351,
FR-33405 Talence, France*

We report on the recent progress achieved in modeling the electronic processes that take place at interfaces between π-conjugated materials in organic opto-electronic devices. First, we provide a critical overview of the current computational techniques used to assess the morphology of organic: organic heterojunctions; we highlight the compromises that are necessary to handle large systems and multiple time scales while preserving the atomistic details required for subsequent computations of the electronic and optical properties. We then review some recent theoretical advances in describing the ground-state electronic structure at heterojunctions between donor and acceptor materials and highlight the role played by charge-transfer and long-range polarization effects. Finally, we discuss the modeling of the excited-state electronic structure at organic:organic interfaces, which is a key aspect in the understanding of the dynamics of photoinduced electron-transfer processes.

1. Introduction: From Conducting Molecular Crystals to Semiconducting Conjugated Polymers

Since the discovery of highly electrically conducting organic materials in the early 1970s,[1−3] charge-transfer complexes made of an electron-donor component (characterized by a low ionization potential) and an electron-acceptor component (with high electron affinity) have played a prominent role in the development of organic conductors, superconductors, and semiconductors.[4] The 1972 synthesis by the group of Cowan of an organic bimolecular crystal in which the electron donor, tetrathiafulvalene (TTF), and the electron acceptor, tetracyanoquinodimethane (TCNQ), form segregated one-dimensional stacks led to an organic material with a high, metallic-like electrical conductivity over a wide temperature window.[5] The conductivity of TTF-TCNQ at room temperature is on the order of 1×10^3 S/cm,[6] that is, similar to that of graphite. These organic molecular crystals provided the proof of concept that, in contrast to the conventional wisdom at the time, organic materials are not intrinsically restricted to be poor electrical conductors.

The intense research efforts triggered by the discovery of TTF-TCNQ followed two major paths. On the one hand, the synthesis in particular by the group of Bechgaard of new molecular crystals based on derivatives of TTF (for instance, those in which sulfur atoms are replaced by

selenium or the TTF moiety is extended by ethylenedithio functionalities) associated with inorganic electrically inert electron acceptors (such as perchlorate or phosphorushexafluoride anions), resulted in the observation of the first organic superconductors.[7] The highest critical temperatures at which superconductivity sets are now in the 10 K range. It is also worth mentioning that in 2001, Kobayashi and co-workers synthesized the first monomolecular crystals with metallic conductivity down to low temperature; in this case, the molecules correspond to a neutral transition metal complex with extended TTF ligands.[8]

On the other hand, efforts focused on π-conjugated polymers. Around Thanksgiving 1976, Shirakawa, MacDiarmid, and Heeger[9] had the idea of subjecting a thin film of the organic polymer polyacetylene, $(CH)_x$, to a redox reaction with either electron donors (reducing agents) such as alkali metals or electron acceptors (oxidizing agents) such as iodine. Remarkably, the formation of the charge-transfer complexes made of, for instance, polycationic polyacetylene chains and iodide anions intercalated in between the chains results in spectacular enhancements of the electrical conductivity; upon increasing level of oxidation or reduction of the polymer chains, the conductivity evolves from some 1×10^{-8} S/cm for pristine polyacetylene up to 1×10^3 to 1×10^5 S/cm.[9] The highest reported conductivities, measured in polyacetylene oxidized by iodine (that is, "iodine-doped" $(CH)_x$ if we were to follow the physics terminology) are on the order of 1.5×10^5 S/cm at room temperature;[10] this value compares well with the

conductivity of copper single crystals, 6×10^5 S/cm. Following polyacetylene, a number of π-conjugated polymers were discovered to become highly conducting upon redox treatment; these comprise polyparaphenylene, polypyrrole, polythiophene, polyaniline, and their derivatives.[11]

Although highly electrically conducting polymers remain of interest for a number of applications as antistatic films, electrochromic displays, transparent electrodes, electromagnetic shielding, actuators, or in the biomedical area,[12] the majority of the research and development efforts since the late 1980s has been devoted to the use of π-conjugated materials (be them molecular, oligomeric, or polymeric in nature) as active elements in semiconductor devices such as organic light-emitting diodes (OLEDs),[13−15] field-effect transistors (OFETs),[16] or photovoltaic cells (OPVs).[17] There as well, the formation of charge-transfer complexes plays a number of useful roles. For instance, Leo and co-workers have demonstrated that the use of oxidants ("p-dopants") or reductors ("n-dopants"), incorporated in the organic material near the interface with the electrode, facilitates charge-carrier injection from the electrode.[18] Also, there is now convincing experimental evidence that the dark current, which directly impacts the achievable open circuit voltage, V_{oc}, in OPVs, originates from thermal excitations of ground-state charge transfer complexes.[19−21] More specifically, it has been predicted that stronger charge-transfer interactions will lower V_{oc} and therefore also the power conversion efficiency of OPVs.[19,22] Note that: (i) the charge transfer at organic interfaces might be either complete (full electron transfer) or partial; and (ii) in both cases, it results in the formation of an interfacial dipole moment that modifies the electronic structure of the components compared to the bulk.

In the instances described above, the charge transfer between the π-conjugated material and its redox partner takes place in the ground state. In what follows, we will deal extensively with organic solar cells and therefore discuss another type of donor−acceptor complexes in which charge transfer is photoinduced and occurs in the excited state. The working principle of organic solar cells has been described numerous times.[23] In contrast to inorganic semiconductors where absorption of a photon at room temperature leads to the generation of free carriers, in the case of organic semiconductors, the photo-generated electron−hole pair remains bound in the form of an exciton (this is the result of the lower dielectric constants of organic materials and of substantial electron−electron correlation and electron-vibration effects). The dissociation of an exciton into separated positive and negative charges (thereby leading to an electrical current) requires that the exciton be able to reach the interface between an electron donor (D) component and an electron acceptor (A) component in the course of its lifetime (typically on the order of nanoseconds for singlet excitons).

The electronic structure, geometric structure, and electric field at the D/A interface all play a critical role in the efficiency of the exciton-dissociation and charge-separation processes, and thus in the efficiency of the organic solar cell. In the simplest picture, the relative energies of the exciton states (be them formed within the donor or acceptor component), charge-transfer states (where an electron [hole] has jumped from the excited donor [acceptor] to a neighboring acceptor [donor]), and charge-separated states (where the electron and hole are far away and completely screened from one another) determine the rates at which charge dissociation or recombination occurs.[24] Depending on the energetics of the donor and acceptor components, additional electronic excited states such as exciplexes (that present mixed molecular-exciton/charge-transfer character) can form upon optical or electrical excitations. Charge-transfer states and/or exciplexes can either: (i) dissociate into charge-separated states (free charges), thereby contributing to the photo-current; or (ii) recombine radiatively to the ground state, which produces light; or (iii) decay nonradiatively into the ground state or into nonemissive states such as triplet excitons. Importantly, the relative orientations of the molecules or the conformation of polymer chains at the interface and their associated electric fields do influence this energetics.

As will be underlined below, modeling the geometric and electronic structures at the interface between organic conjugated materials remains a formidable task that has so far received only limited attention. Yet, the results that have been reported point to the key role of interfacial effects in the electronic and optical processes taking place in opto-electronic devices. Here, we review some of these works with a special focus on (i) the simulations of the local geometric structures at organic:organic interfaces (section II); (ii) the electronic effects triggered by the differences in the chemical structures of the donor and acceptor components across such interfaces (section III); and (iii) the nature and fate of electronic excited states at organic:organic interfaces (section IV). Throughout the review, we highlight how such interfacial effects can affect the efficiency of the charge-separation and charge-recombination processes occurring in OLEDs and OPVs.

2. Modeling the Geometric Structure at Organic:Organic Interfaces

The modeling of organic donor−acceptor interfaces, i.e., the theoretical description of their morphology under given thermodynamic conditions (including temperature and composition), can easily be viewed as one of the most challenging tasks to be tackled by computational physical chemists. While such a modeling is now becoming more achievable thanks to a combination of methodological improvements and increase in computational resources, it should come as no surprise that very few articles dealing with organic:organic (O:O) interfaces have appeared to date. Indeed, the modeling of n-type/p-type (acceptor/donor) interfaces introduces several technical challenges that can easily hamper the feasibility and reliability of the computational approach.

Issues. In contrast to inorganic:inorganic (I:I) p−n interfaces (and to some extent to I:O hybrid junctions)

where strong covalent and ionic forces are in play, the very nature of the O:O interfaces is dominated by a combination of weak van der Waals dispersion forces, electrostatic interactions, and steric repulsions acting between the often flexible small molecules or macromolecules composing the system.[25] Consequently, not only in the bulk crystalline phase of organic compounds,[26] but even more so at their interfaces, the free energy landscape becomes a very complex function of the atomic positions, characterized by the presence of several local minima with very similar energy. This issue could be referred to as thin-film or interface polymorphism, because the crystalline structures present only at interfaces are sometimes named thin-film polymorphs.[27,28]

The existence of a range of free energy minima and the solid nature (crystalline or more often glassy) of the components at room temperature imply that, once the interface is formed, its structure remains generally fixed as evolution to a lower free-energy state is difficult. Hence, for a given donor−acceptor system, the interface morphology is not unique and depends on the preparation techniques (in fact, not only in experiments but also in simulations) through a subtle balance of thermodynamic and kinetic effects.

Within the same donor−acceptor system, the local nature of the interface can vary at different levels including degree of crystallinity and commensurism, direction of epitaxy, polymorphism, roughness and dimension of the interfacial region, size of the acceptor and donor phases, presence of grain boundaries and shape of the grains, or contamination with solvent molecules. All these properties are affected not only by the chemical nature of the components but also by the technique of preparation of the interface (e.g., solution or vacuum processing), temperature of the substrate/stage, concentrations and types of solvents and additives, order and speed of deposition/casting, and annealing temperature and time. This makes it very difficult to control and obtain the desired morphology (see ref 29 for a illustrative example regarding P3HT/PCBM solar cells).

Since the detailed nature of the interfacial morphologies strongly impacts the electronic properties at the D/A interface, the modeling of O:O heterojunctions requires the identification of essential model parameters as well as the incorporation to some extent of factors mimicking the preparation technique experimentally used for the system under study. In the following, we critically review the existing techniques and details of modeling and suggest guidelines for future work in the field.

Computational Techniques. The computational techniques used for simulating I:O interfaces start to be employed also for modeling O:O systems. They include potential-energy minimization methods, PE,[30,31] in particular molecular mechanics (MM), and free-energy minimization methods, such as molecular dynamics (MD) and metropolis Monte Carlo (MC).[32] Kinetic Monte Carlo methods (KMC) have also shown their usefulness for simulating crystal-growth dynamics;[33−35] however, they need to be complemented by PE or MD/MC methods for the calculation
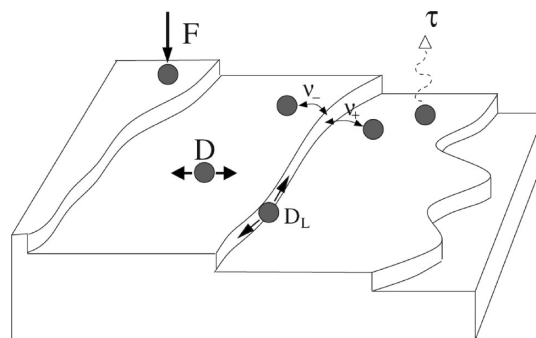

Figure 1. Summary of various atomic processes on a vicinal surface. Deposition with a flux F, diffusion with D as the diffusion constant, desorption with rate $1/\tau$, and step attachment or detachment with rate $\nu\pm$ from each side is shown. D_L represents the line diffusion along the step. Reproduced with permission from ref 33. Copyright 2010 American Physical Society.

of the overall energetics. For a detailed description of all these methods, excellent textbooks and reviews are available.[36−39]

Independently of the details of the model, MD is in general preferable over Monte Carlo methods because, by using ad hoc configurations updates, it provides the "true" dynamic evolution of the system and allows the treatment of both nonequilibrium and equilibrium situations, as well as the evolution from one case to the other. More importantly with respect to the calculation of the electronic properties, MD produces the trajectory of the system coordinates, which is required to take into account the impact of dynamical fluctuations on these properties.[40−42] However, currently, MD simulations are applicable to relatively small samples on the order of $\sim 1 \times 10^5$ atoms for time windows on the order of ~ 100 ns; where MD simulations are not feasible, methods relying on more drastic approximations such as KMC come into play. KMC is particularly appealing as it introduces a stochastic time variable into the MC simulations for the rates of the processes that are known (for instance, adsorption or desorption in Figure 1); in contrast to MD, the processes are run on an artificial trajectory and much longer time scales can be followed. KMC is, for instance, very useful to study the process of crystal growth from vapor deposition. A very good example is the work of Choudhary et al.,[34] where the growth of pentacene on several inert substrates was studied; KMC makes possible the derivation of a schematic phase diagram as a function of the interaction with the substrate and of the flux intensity (Figure 2). Another interesting example at the atomistic level is the growth of a C_{60} phase on graphite;[35] the work of Liu et al. is stimulating as it couples the use of MD for the computation of the process rates, notably the diffusion of uppermost C_{60} molecules from a lattice site to another, with KMC for the simulation of the growth. This combination of techniques is promising and has been demonstrated to be applicable also to growth from solution.[43]

It is worth stressing that the MC method is in principle equivalent to MD in terms of structural data and, thus, of the quality of the final morphology. However, it presents
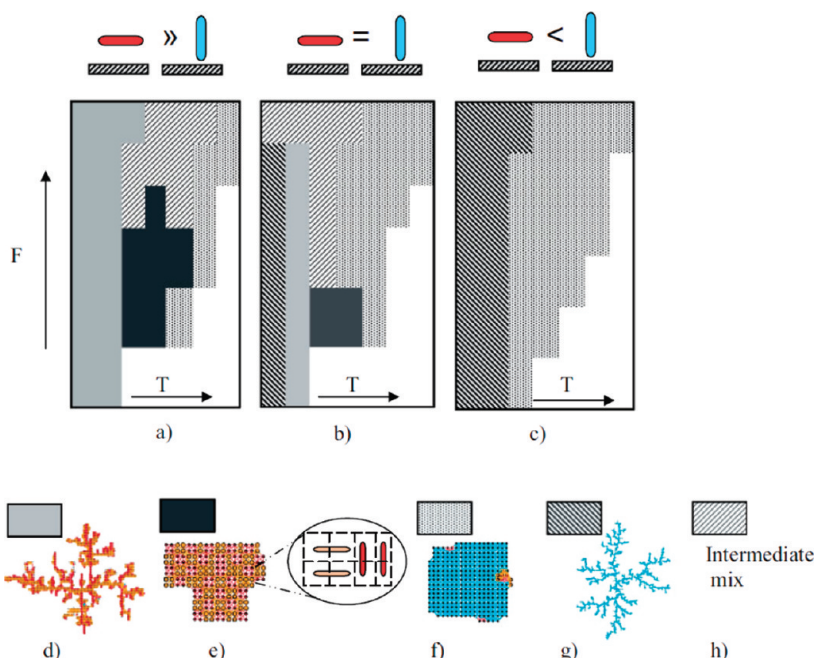
Figure 2. Morphology diagram of pentacene molecules on various substrates calculated using KMC simulations using a color code representative of different growth morphologies. For example, gray represents the regime characterized by dendritic growth with an orientation parallel to the substrate. Here, F is the rate of the deposited molecules and T is the temperature of the substrates. The morphology diagrams are given as follows: (a) when molecule−substrate interactions favor parallel rather than upright orientations; (b) when molecule−substrate interactions in both orientations are similar; (c) when molecule−substrate interactions in an upright orientation are larger than those in a parallel orientation. Color coded representations of different growth morphologies are: (d) gray, all molecules lie parallel to the substrate and are characterized by a dendritic arrangement; (e) black, compact formation with all molecules parallel to the substrate; (f) light-gray dots, compact structure with the majority of the molecules in a perpendicular orientationl (g) dark-gray diagonal lines, dendritic structures in which the majority of molecules lie in perpendicular orientations; (h) light-gray diagonal lines, transitional structures, which could not be classified as belonging to any distinct group.

technical drawbacks due to the difficulty of encoding efficient MC moves in the case of flexible molecules; as a result, it is only applicable to simple systems such as lattice[44] or coarse-grained[45] models. This difficulty is compensated by the possibility it provides of attempting unphysical moves, such as altering the connectivity along a polymer chain, which allows fast equilibration in bulk polymer simulations.[46] Unfortunately, the advanced MC techniques exploited for studying conventional polymers such as polyethylene or polystyrene remain to be developed to investigate D/A polymer blends; they will certainly find useful applications in the near future.

Although PE methods appear to be the worst possible choice for simulating O:O interfaces in terms of accuracy of the final results, their limited computational requirements make them useful, for example, to investigate commensurism between an organic surface and an organic overlayer.[31] The main drawbacks of PE methodologies are the neglect of entropic and thermal effects (the temperature is set to 0 K) and the inability of moving from an energy minimum of the system to another. The search for global minima therefore requires the exploration of the full parameter space, which may not be feasible if the space is too large. In practice, the technique is applicable only for crystalline systems of known−or assumed− elementary cells; in this case, surface energies can be calculated and the relative orientations and positions of the two cells at the interface can be optimized. The need of knowing the crystal structures makes PE a good technique to complement experimental measurements; this has

been shown with MM calculations by Campione et al. in the analysis of rubrene−quaterthiophene and rubrene− tetracene interfaces generated by organic molecular beam deposition,[47,48] or by Verlaak et al. in the optimization of the relative positions of two large, finite crystalline islands to represent the pentacene(001)/C_{60}(001) and pentacene-(01$\bar{1}$)/C_{60}(001) interfaces.[49]

When the unit cells and epitaxial relations are known for crystalline interfaces, an "isolated complex" approach can be considered. In such an instance, a donor and an acceptor molecule are placed in a few meaningful geometries and the opto-electronics properties can be calculated at the quantum-mechanics (QM) level. Although such "isolated complex" studies are useful for understanding the main processes occurring at the interface (see refs 50−53 and the following sections), they cannot generally provide quantitative predictions since they neglect the positional/thermal disorder at the interface (see Figure 3) as well as cooperative effects such as polarization.[42,49,54] A further step toward a more realistic description of the interface is represented by QM studies of clusters of molecules on a well-defined crystalline structure, such as the investigation performed by Linares et al.[55] on the pentacene(01$\bar{1}$)/C_{60}(001) systems. In general, the time has come for definitely going beyond "isolated complex" studies through more detailed modeling of interface morphologies based on the combination of QM, MD, and KMC techniques.

Level of Modeling. Different complexities of modeling have been attempted to describe O:O interfaces, from
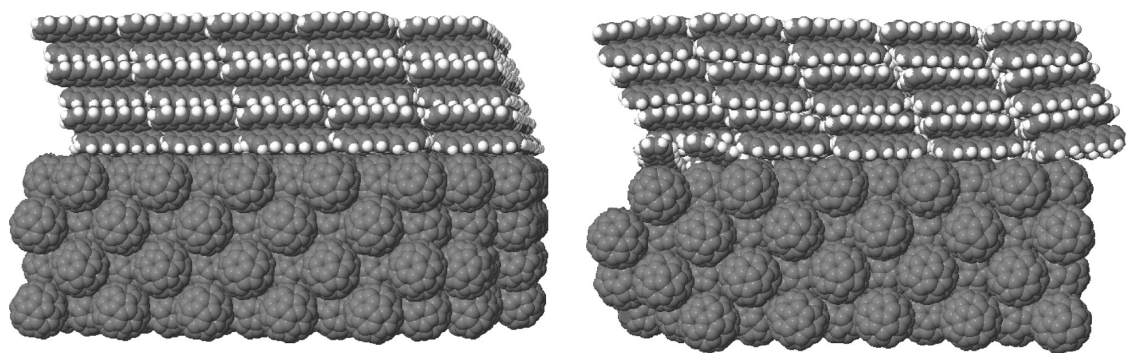
Figure 3. Portion of a pentacene(01−1)/C60(001) supercell with fixed crystal structure, as used in ref 49, and a similar structure equilibrated with MD at 500 K. The comparison reveals the extent of the thermal disorder and the different types of results that can be obtained using the PE or the MD technique.

lattice to atomistic approaches. Expectedly, it is found that the simpler the model, the longer the simulation time scales and the larger the dimension of the system that can be handled. Unfortunately, for the calculation of the relevant electronic properties with computational chemistry methods, which is the main subject of this Review, the only useful models are the ones with explicit atomic details or with precise mapping of the atomic positions.[56] However, it is of interest to consider the various levels of description, in particular with the view of eventually bridging them together on a multiscale platform to model devices from first principles, i.e., to predict the performance of devices on the sole basis of the chemical structure of their constituting materials and their morphologies.

Lattice models (LM) have been used up to now to produce qualitatively meaningful morphologies in several studies targeting the simulation and optimization of solar cell devices.[44,57−63] These are usually inspired from the Ising Hamiltonian adapted to reproduce phase separation during binary film coevaporation.[64] Despite its usefulness for understanding solar cell performance as a function of the extent of phase separation between the two components, this approach is very limited in terms of morphology, as only a few parameters link the model to reality (namely, the size of single-component lattice domains ("spins"), the interaction between unlike spins, and the temperature). LM-based solar cell simulations require the knowledge of several material parameters to give realistic results (dielectric constants, charge mobilities, exciton transfer rates, recombination rates). In the quest for a multiscale approach, it is highly desirable to be able to compute these parameters from first principles before proceeding to device simulations.

Coarse-grained models (CGM) have also earned some success in the modeling of O:O interfaces. They can be roughly classified into two categories, generic and specific models. Generic CGMs do not aim at describing a specific molecule but a category of molecules;[65] consequently, the mapping from model to atomic positions cannot be realized, at least not completely, and the electronic properties cannot be calculated at a quantum-chemistry level. Their usefulness comes from their ability to point to general trends. Recent studies have reported, for instance, the consequences of confinement on polymer chains,[66]

the growth of pentacene on model surfaces,[34] the role of various charge distributions on the phase organization of discotic semiconductors,[67] the phase behavior of donor−acceptor liquid crystalline compounds,[68] the anisotropy of energy transfer[69] or charge mobility in liquid crystals,[70] or the exciton transport in perylene-end-capped oligofluorenes.[69]

Specific CGMs have instead the ambitious target of reproducing atomistic modeling results while using a simpler potential energy function.[56] This simplification is often possible for both small molecules and polymers, but requires a tedious parametrization work;[56,71,72] thus, such a CGM is usually effective only in the specific conditions or for the specific properties it has been derived. As a practical consequence, the effort is rewarding only if the chosen system is of general interest. It is then not surprising that the few studies that have been reported dealt with protypical systems such as perylene or naphthalene tetracarboxy-dianhydrides (PTCDA/NTCDA) and copper phthalocyanines.[73,74] To the best of our knowledge, the only investigation in the field of O:O interfaces relates to the coarse-graining modeling of P3HT/C60 mixtures performed by Huang et al.;[72] in this work, a first demonstration of the phase separation of the two compounds by cooling a liquid mixture was reported (see Figure 4).

Finally, atomistic models represent to date the best approach both for describing a specific system and for the quality of the subsequent calculations of the electronic properties from the simulated morphologies. These higher levels of specificity and detail come of course at a higher computational cost. This limits the system size and time scales to such an extent that the treatment of some materials, namely polymers, becomes unpractical; in such cases, it is necessary to rely on CGM approaches[56,71] or to restrict the study to oligomers.[75] For small molecules used in the field of organic electronics, the reliability of the results has been demonstrated in several instances (see, for example, refs 40,75−81), often in tandem with electronic-structure calculations.[40,75,79,80] Investigations involving explicit modeling of O:O interfaces is much less abundant but of great interest. We can mention the joint experimental−theoretical study of Raos and co-workers on the deposition of quaterthiophene on a potassium hydrogen phthalate single crystal;[77,78] the work of Martinelli et al.
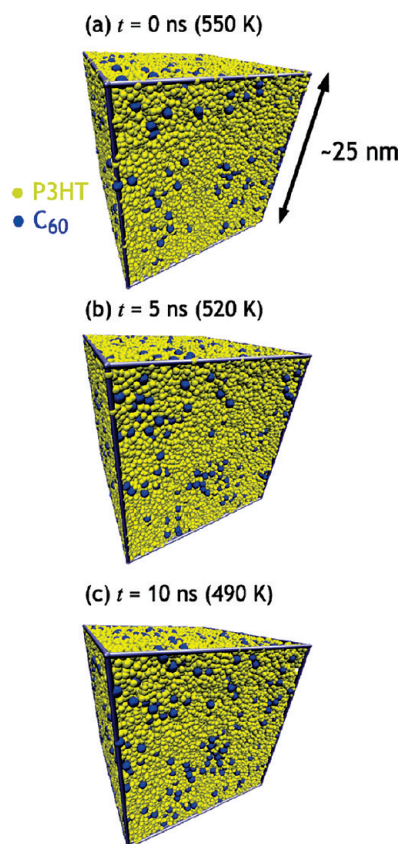
Figure 4. Snapshots from a constant NPT CG simulation of 768 P3HT 48-mers (MW about 8 kDa) and 4608 C60 molecules (1.85:1 w/w P3HT: C60, 115 200 particles) in which the system is cooled from 550 to 490 K over a period of 10 ns (the system is periodically replicated in all three directions). The initial configuration consisted of randomly placed chains and fullerenes. P3HT and C60 particles are in yellow and blue, respectively. Reproduced with permission from ref 72. Copyright 2010 American Chemical Society.

on polymer/pentacene interfaces, which provides a useful insight on the effect of the dielectric on charge-carrier mobilities in OFETs;[41] the study by Zheng et al. on the phase separation of C_{60} and pentacene;[82] or the interesting works of Clancy and co-workers on several processes occurring during the growth of organic crystals, in particular for pentacene.[83-85] The latter papers complement, with a totally different approach, the results shown in refs 49,55.

It is worth mentioning that many of these investigations use, instead of a fully atomistic approach, a slightly simplified version, i.e., the so-called united-atom approximation. This approach consists of an implicit modeling of the hydrogen atoms that are combined as a single site together with the heavier atoms they are bonded to (for organic molecules, this often means carbon atoms with a specific hybridization). This approximation (which could be viewed as an optimal CGM) can be recommended: although it reduces both the number of centers and the integration step to about one-half (organic molecules contain about 50% of H atoms, and C−H stretchings are the fastest motions in the systems), it retains the same level of quality as the full atomistic approach in the reproduction of molecular organizations and static physical properties. With respect to the dynamics of the system,

the united-atom approximation, with its smoothing of the exposed surface, generally leads to an acceleration of molecular motions; this feature is beneficial for equilibration but has to be kept in mind if absolute values of correlation times are to be predicted.[86]

3. Modeling the Ground-State Electronic Structure at Organic:Organic Interfaces

As emphasized in the Introduction, a comprehensive description of the charge-photogeneration mechanism in organic photovoltaic cells implies the detailed knowledge of the electronic structure at the heterojunction between the donor and acceptor materials. It is now well established that, provided the electronic structures of the donor and acceptor materials are properly tuned, excitons that reach the donor−acceptor interfaces can undergo a dissociation process to a charge-transfer (CT) excited state with a hole on the donor and an excess electron on the acceptor. However, how the positive and negative charges can escape from their Coulomb attraction to produce separated free charge carriers remains an open question. Two main mechanisms have been proposed to describe the charge-separation process, a "hot CT state" mechanism and an electric-field assisted mechanism (see, for instance, ref 87; we will come back to the former mechanism later in this Review). In the latter, the charge-transfer states first fully thermalize and subsequently break up into free charge carriers with the help of local electric fields at the interfaces.[88] These interfacial electric fields are believed to arise from interfacial dipoles (due to possible ground-state partial charge transfer and to polarization effects resulting in redistributions of the electronic clouds over the donors and acceptors) and from the (small) built-in electric field. Ultraviolet photoelectron spectroscopy (UPS) measurements have provided direct evidence for the existence of significant dipoles at the interface between organic materials.[89−93]

In this context, the development of modeling approaches to identify the origin and magnitude of interface dipoles and to assess the state-energy landscape at organic D/A heterojunctions is an important step toward the rationalization and optimization of power conversion efficiencies in organic solar cells. However, theoretical works addressing these issues remain scarce, which is mainly due to the lack of precise information regarding the molecular organization at the interface (as discussed in section II), whereas several experimental studies have demonstrated the crucial role of the interface morphology on the energy landscape in organic:organic heterostructures.[94−97] Moreover, although the description of well-ordered interfaces is tractable by means of QM calculations carried out on infinite systems using periodic boundary conditions, these approaches are not relevant for the O:O interfaces we are interested in, as they present a high degree of positional disorder.

Long-Range Electrostatic Effects. To include explicitly the contributions from long-range electrostatic interactions to the ground-state electronic structure at O:O

interfaces, we recently developed a multiscale modeling approach including complementary microelectrostatic (ME)[98,99] and quantum-chemical methods.[55] Although a quantum-chemical description provides a quantitative picture of the electronic structure at the interface without adjustable parameters, the parametrized ME approach, in which molecules are coarse-grained into electrical multipoles, is useful to study large-scale clusters. This modeling scheme has been applied to the pentacene/C_{60} interface, chosen as an archetype for bulk heterojunctions between small donor molecules and electron-acceptor fullerene-type molecules, in order to calculate the quadrupole-induced interface dipoles (QIDs) and the energy profile normal to the interfacial dissociation zone. An intriguing peculiarity of the pentacene/C_{60} heterojunction is the discontinuity of the quadrupolar field that varies abruptly across the interface, as a result of the presence of a large permanent quadrupole moment in pentacene molecules and its absence in spherical C_{60} molecules.

Cofacial arrangements of pentacene/C_{60} complexes were first investigated using correlated ab initio and density-functional theory (DFT) methods to address the origin of the interfacial dipole moment in these heterojunctions. For intermolecular distances larger than 3 Å, the charge transfer between the two molecules is very weak, and the interface dipole mostly results from polarization effects. It was also shown that the orientation of the interfacial dipoles depends on whether the C_{60} center-of-mass is located on top of the pentacene molecular backbone, or at the edge of the pentacene molecule. This effect can be traced back to the uncompensated quadrupolar field at the interface. The pentacene quadrupole can be viewed as the result of a collection of 14 CH units that are polarized with negative partial charges on the inner carbon atoms and positive partial charges on the outer hydrogen atoms. When the C_{60} molecule mainly interacts with the π-electronic density of the carbon atoms of pentacene, the reorganization of the electronic cloud over the fullerene molecule promotes a sizable intramolecular charge transfer away from pentacene. Interactions with the hydrogens atoms of pentacene generate the opposite polarization of C_{60}, as illustrated in Figure 5.

Model interfaces of increasing complexity have then been investigated using either a microelectrostatic coarse-grained representation of the pentacene and C_{60} molecules or a valence-bond/Hartree−Fock (VB/HF) method.[55] The VB/HF model[54] involves a self-consistent-field procedure in which the orbitals of the system under investigation are optimized with the constraint to be confined over a single molecular unit. This allows the calculation of the electronic properties of a given fragment embedded in a larger stack, while including explicitly the polarization effects induced by intermolecular electrostatic interactions. Moreover, because of the local nature of the orbitals, the VB/HF scheme also allows specific assignments of the electrons over various molecular fragments. Calculations carried out on neutral molecular assemblies
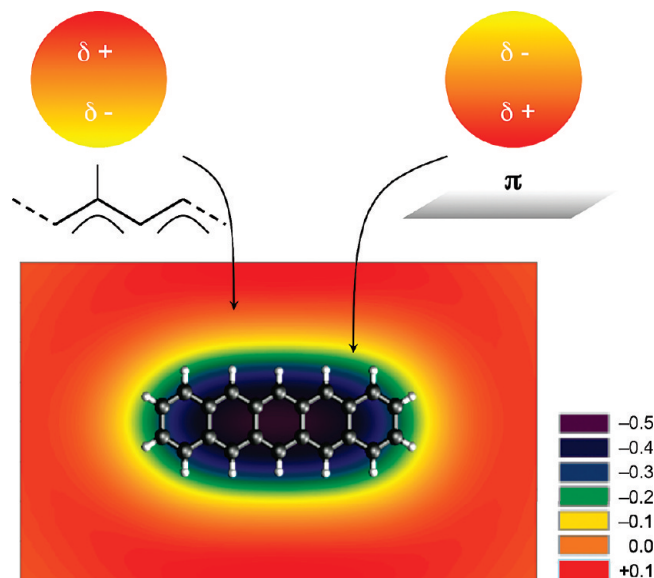

Figure 5. Interface dipole moment (in Debye) of the pentacene/C_{60} dimer as a function of the degree of translation of the C_{60} molecule parallel to the pentacene plane, as calculated at the AM1 level.

thus involve the strict electroneutrality of each molecular fragment (which is consistent with the negligible intermolecular ground-state charge transfer inferred from correlated ab initio calculations on pentacene/C_{60} complexes[55]), a feature which is also implicit in the ME approach. As an example, Figure 6 illustrates the variation of the induced dipole moment (calculated at the VB/HF level) on a single C_{60} molecule interacting with a pentacene surface corresponding to the $(01\bar{1})$ plane of the single crystal.

The ME model was used to characterize the molecular dipoles generated at the pentacene$(01\bar{1})$/$C_{60}(001)$ interface in a disklike molecular cluster around the interface (with a radius of 10 nm and a thickness of roughly 6 nm), see Figure 7. Figure 7 also illustrates the distribution of the dipole moments on the pentacene and C_{60} molecules in the vicinity of the junction between the two molecular materials (blue arrows), whereas the red arrows on the left part represent the dipoles averaged over each monolayer. These results show that the quadrupole-induced dipoles are extremely sensitive to the topology of the interface and hence to the nature of the environment around each C_{60} molecule. Importantly, they also underline that the averaged dipoles do not provide a suitable description of the local electric fields felt by the individual molecules. This is particularly clear when comparing the averaged interface dipole over the first monolayer of C_{60} molecules, which points toward the pentacene side, to the individual molecular induced dipoles that display alternations in their orientation along the interface. An implication of these results that must be borne in mind is that UPS measurements, because of their microscale resolution, can only reflect the average value of the interface dipole and thus completely overlook the nanoscale variation of the electronic interactions.

Opto-electronics devices such as photovoltaic cells typically involve so-called 'type II' heterojunctions[100] where, in a simple one-electron picture, both the highest
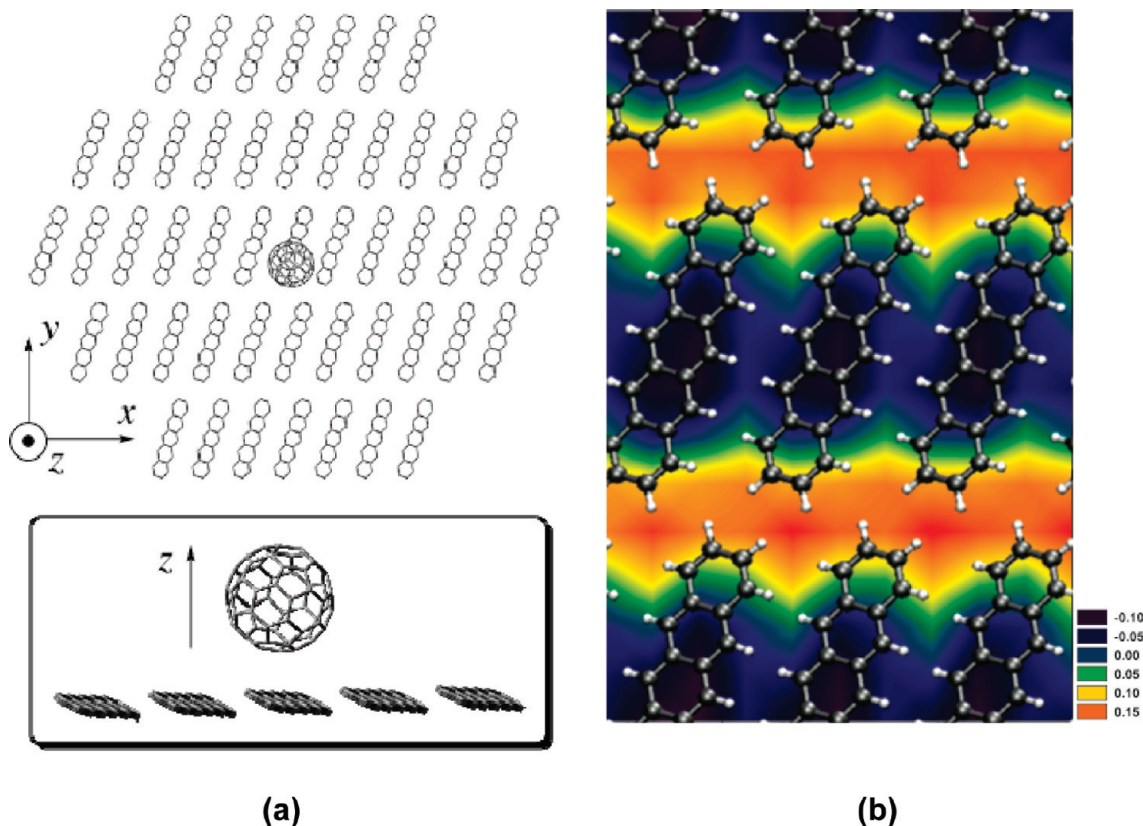
Figure 6. (a) C_{60} molecule above a plane of pentacene units, and amplitude of the z-component of the induced dipole on the C_{60} molecule as a function of its position on the (x, y) plane, as calculated using the VB/HF-AM1. Reproduced with permission from ref 55. Copyright 2010 American Chemical Society.
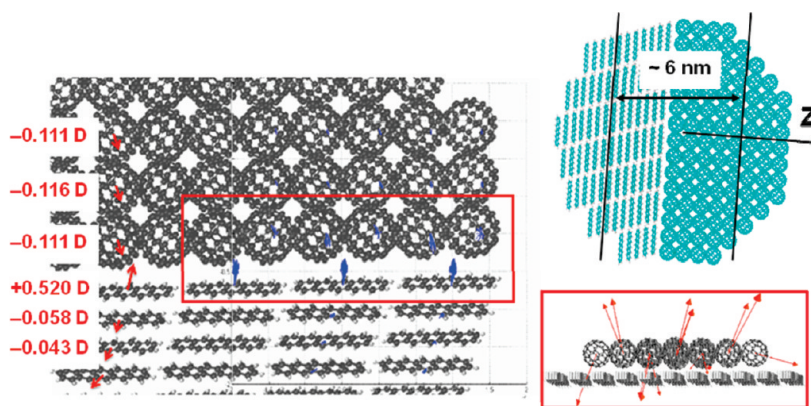

Figure 7. Quadrupole-induced dipoles at the pentacene(01−1)/C_{60}(001) interface: individual induced dipoles (blue) and layer-averaged induced dipoles (red), as calculated using the microelectrostatic model (left). The dispersion of the induced dipole moments on the C_{60} molecules at the interface is highlighted in the inset (bottom right). Adapted with permission from ref 55. Copyright 2010 American Chemical Society.

occupied molecular orbital (HOMO) and lowest unoccupied molecular orbital (LUMO) levels of the donor lie higher in energy than the corresponding levels on the acceptor. Depending on the actual energy mismatch between the frontier orbitals, type II heterojunctions can either facilitate charge separation, which is exploited in photovoltaic cells,[101−103] or trigger energy transfer and enhance quantum yields, which is exploited in light-emitting diodes.[100,104,105] It must be stressed that such simple HOMO−LUMO diagrams should be considered with much caution, as they rely on the electronic structure of the bulk donor and acceptor materials and thus completely neglect interfacial effects. In particular, the occurrence of an interfacial dipole

moment results in a "vacuum level shift" (VLS) that can significantly alter the relative positions of the donor and acceptor molecular orbitals, as schematically shown in Figure 8. In the classical approximation, the VLS writes:

$$\text{VLS} \approx - \sum_i \frac{\mu_z^i}{\varepsilon \varepsilon_0 S} \quad (1)$$

where μ_z^i is the component of the dipole moment of molecule i along the direction perpendicular to the interface, ε the relative dielectric constant, and S the surface area occupied by the molecule at the interface. In the case of the pentacene(01$\bar{1}$)/C_{60}(001) interface modeled at the

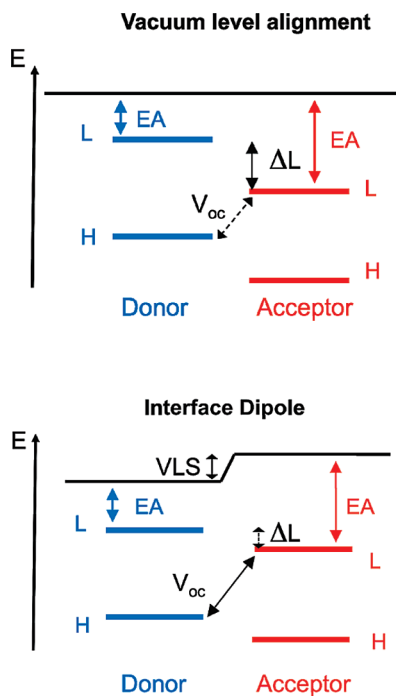**Vacuum level alignment**

Interface Dipole

Figure 8. Energy diagrams of the frontier electronic levels in a donor/acceptor complex, in the absence (top) and in the presence (bottom) of an interface dipole.

ME level, a VLS value of ~0.11 eV has been estimated from eq 1;[55] this is in very good agreement with the measured VLS values.[106]

Interestingly, a reversal in the polarity of the VLS has been observed experimentally upon inverting the deposition sequence for pentacene/C_{60} interfaces.[106] Also, by using a combined experimental (UPS)/theoretical (DFT) investigation, Koch and co-workers have shown that the ionization potential of a pentacene layer can vary by as much as ~0.6 eV when going from a layer where the molecules lie flat on the substrate to a layer where they stand up.[94] To assess in a more quantitative manner the impact of molecular orientations on the electronic structure across the interface, Verlaak et al.[49] have performed ME calculations on two different pentacene surfaces interfaced with a C_{60} (001) surface: the pentacene (01$\bar{1}$) surface which is characterized by a high density of π-orbitals exposed to the surface, and the pentacene (001) surface which exposes the C−H bonds to the surface (see Figure 9). Here, the VLS has been computed more directly from the variation of the charge−QID interaction energy as a charge crosses the interface. The results are reported in Figure 9 for the hole−QID interaction energy (which is equal in magnitude but opposite in sign to the electron−QID interaction). A remarkable difference is noticeable when comparing the vacuum level shifts of the two interfaces studied. As a result of the different orientations of the pentacene molecules relative to the interface, the sign of the VLS reverses when going from the pentacene(001)/C_{60} to the pentacene (01$\bar{1}$)/C_{60} interfaces. Thus, different crystal orientations lead to differently oriented QIDs and in turn to a reversed polarity of the VLS.

The energetic landscape for dissociation of geminate pairs at the pentacene/C_{60} interface has also been investigated

using the ME model. When collecting all bulk and interfacial contributions to the energetics of free charges in pentacene/C_{60}, the transport level energies for positive and negative charge carriers can be evaluated[49] and result in the energy diagrams shown in Figure 9. As expected, the more electrostatically "reactive" pentacene(00$\bar{1}$)/C_{60} interface displays more substantial deviations from the simple level alignment picture than the more "inert" pentacene(011)/C_{60} interface. In particular, the electrostatic interactions between the negative charge on C_{60} [positive charge on pentacene] and the quadrupolar field at the interface drive the charge away from the pentacene-(01$\bar{1}$)/C_{60} interface. In a simplified view, an excess electron on a C_{60} molecule lying close to the pentacene(01$\bar{1}$) surface feels the repulsive interaction induced by the π-electronic cloud of the facing pentacene molecules, and is therefore destabilized in comparison to the bulk. The same holds true for an excess positive charge lying on a pentacene molecule at the same surface due to the uncompensated quadrupolar field.

Applying the same ME approach to geminate pairs with increasing electron−hole separation across the interface, the electrostatic energy landscape for charge dissociation can be built. The results of these calculations indicate that an energy difference of ~0.4 eV needs to be overcome to split the geminate pairs into separate charges in the case of the pentacene(011)/C_{60} interface; in other words, recombination of the electron−hole pairs can be favored over separation in this configuration. In contrast, the geminate pair is equally stable as the separated charges for the pentacene(01$\bar{1}$)/C_{60} interface, so that geminate pair splitting could easily occur. However, the complexity of the charge-separation mechanism can be highlighted when comparing these results with the results of quantum-chemical calculations of the exciton-dissociation and charge-recombination rates performed on isolated pentacene/C_{60} complexes;[52] in these studies, the charge-recombination rates are calculated to be several orders of magnitude larger in a complex with a parallel configuration (mimicking the pentacene(01$\bar{1}$)/C_{60} interface) than in a complex with a perpendicular configuration (mimicking the pentacene(011)/C_{60} interface). These conflicting features again underline the need for the development of multiscale approaches.

Finally, we note that the microelectrostatic calculations referred to above do not distinguish between singlet and triplet states. Because the exchange interaction is small compared to the Coulomb attraction in charge-transfer pairs,[107] we expect the energy diagram of Figure 9 to be essentially spin independent; thus, the scenario for the splitting of the bound pairs is expected to be equally valid for triplets. In this context, it has been recently suggested that the large diffusion lengths and low open-circuit voltage measured for pentacene-based solar cells are associated with triplet excitons generated from singlet fission.[108]

Ground-State Charge Transfer. The formation of an interface dipole at O:O interfaces can be triggered by polarization effects (i.e., reorganization of the electronic density *within* the molecules across the interface), as
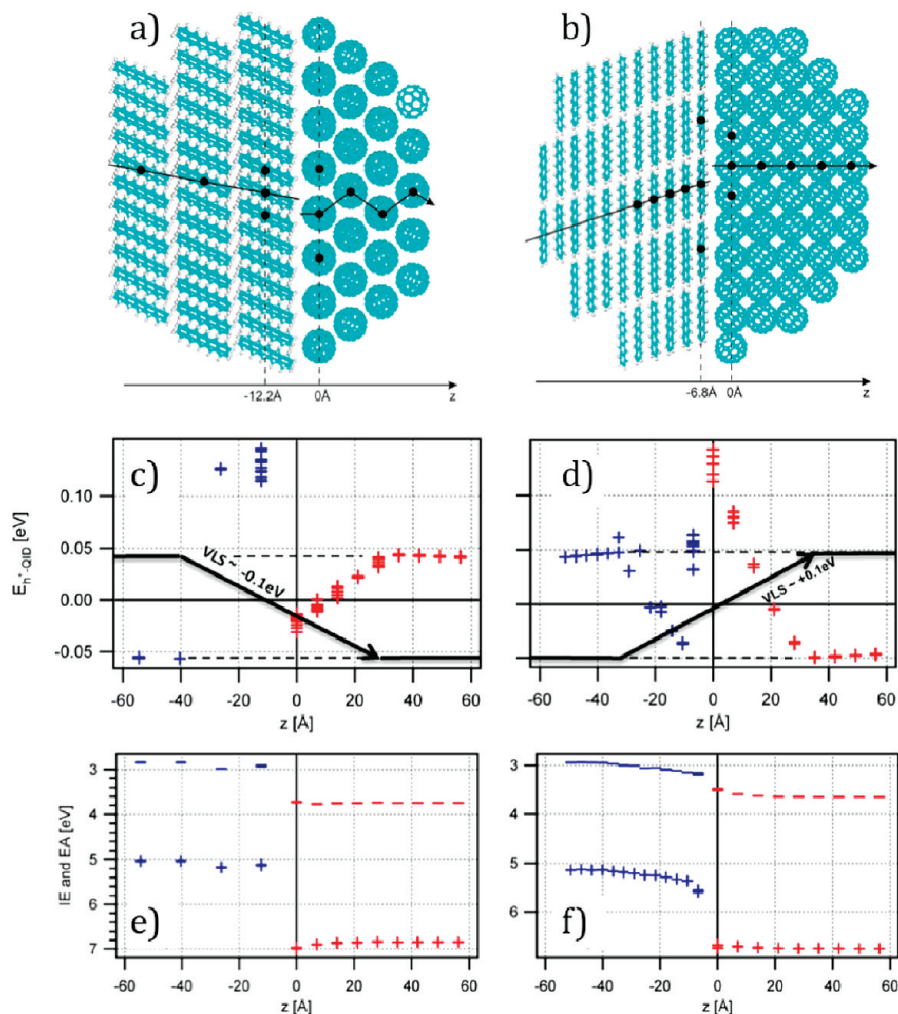
Figure 9. Top: (a) Pentacene(001)/C_{60}(001) interface and (b) the pentacene(01−1)/C_{60}(001) interface. The black dots denote the molecules for which simulation results are shown. Middle: Hole-QIDs interaction energy (eV) near (c) the pentacene(001)/C_{60} interface; (d) the pentacene(01−1)/C_{60} interface. Each "+" represents the hole−QID interaction energy for the hole on a molecule with the corresponding z-value. Bottom: Computed energy diagrams of (e) the pentacene(001)/C_{60} interface and (f) the pentacene(01−1)/C_{60} interface. Adapted with permission from ref 49. Copyright 2009 Wiley.

discussed above, as well as by (partial) charge transfer between the donor and acceptor units. A charge transfer requires the overlap between the molecular orbitals of the two molecules in contrast to the long-range polarization effects. A general quantum-mechanical theory of ground-state charge transfer has been developed in the seminal work of Mulliken to explain color changes induced when mixing together two or more chemical species.[109] The theory relies on the formation of complexes between electron acceptors and donors (Lewis acids and bases) stabilized by resonance interactions between the covalent ground state and ionic charge-transfer states. In the simple case of a single donor−acceptor (D−A) pair and a basis set including only the diabatic configurations $|DA\rangle$ and $|D^+A^-\rangle$ (neglecting the higher-energy $|D^-A^+\rangle$ configuration) built from the product of the spin-adapted wave functions of the separated donor and acceptor molecules in their neutral and charged ground states, quantum-mechanical coupling between D and A yields the following two adiabatic electronic states:

$$|\psi_{GS}\rangle = a|DA\rangle + b|D^+A^-\rangle$$
$$|\psi_{CT}\rangle = c|D^+A^-\rangle + d|DA\rangle \qquad (2)$$

where $a \gg b$ and $c \gg d$ for weakly coupled donor−acceptor pairs. From first-order perturbation theory, the coefficients in eq 2 are proportional to the matrix elements $\langle DA|H_{DA}|D^+A^-\rangle$ (where H_{DA} is the donor−acceptor interaction Hamiltonian) and inversely proportional to the corresponding energy difference, $E_{DA} - E_{D+A-}$. Note that, provided the amount of mixing in eq 2 is large enough, an intense intermolecular charge transfer transition from $|\Psi_{GS}\rangle$ to $|\Psi_{CT}\rangle$ is predicted that primarily involves the state dipole moments in the $|DA\rangle$ and $|D^+A^-\rangle$ configurations.[109] As a result of this mixing, the electronic ground state acquires a partial charge-transfer character, thus corresponding to a fraction of $|e|$ transferred from the donor to the acceptor. A simple way to predict the possibility of charge transfer between the two moieties in the excited state is to analyze the delocalization of the wave functions in neutral complexes.[110]

At this stage, it is useful to say a few words on the induced density of interface states (IDIS) model that has been used extensively in the literature to describe the amplitude and direction of charge transfer at O:O interfaces.[111] The key feature of this model is to associate to a given organic semiconductor a quantity referred to as

the charge neutrality level (CNL). The latter is experimentally determined by depositing the molecular semiconductor on a nonreactive surface; this adsorption leads to a broadening of the discrete molecular levels upon hybridization with the orbitals of the metal atoms. The CNL is obtained as the energy at which the integrated density of states over the molecular component amounts to the number of electrons in the molecule. The CNL is a quantity that appears to be robust when changing the nature of the metal or the contact geometry. It has to be seen as equivalent to a "Fermi level" of the molecule that will govern the direction and amplitude of the charge transfer at the organic/organic interface: The charge transfer should occur in such a way as to equalize the CNLs of the two molecules, leading to a potential drop equal to $S_{00}(CNL_1 - CNL_2)$. Here, S_{00} is a screening parameter that accounts for the polarization of the medium upon charge transfer and is usually expressed in terms of the static dielectric constants of the two materials. Note that the pillow effects characteristic of metal/organic interfaces[112] and linked to Pauli exchange effects at the interface are generally neglected at organic/organic interfaces because of the smaller interfacial electronic density.

Although the IDIS model proved useful to predict and rationalize the interface dipole as measured by UPS spectroscopy at O:O interfaces,[113] it introduces conceptual issues and limitations that call for more advanced approaches. In particular:

(i) The CNL level relies on the broadening of the electronic levels at metal/organic interfaces, even though such a broadening is not expected to occur at O:O interfaces.[114]

(ii) The IDIS model suggests that the direction and amplitude of the charge transfer depends only on the difference between the CNL levels of the two molecules. However, it is well-established that the electronic coupling between two orbitals is highly sensitive to the relative positions of the two interacting molecules.[115] For instance, an increase in intermolecular separation yields an exponential decrease in electronic coupling due to the reduction in orbital overlap.[116] That the sole consideration of chemical potentials cannot fully predict the amplitude of charge transfer has been further illustrated in the case of metal/organic interfaces.[117] This suggests that the IDIS model might be more appropriate when considering a micrometer scale (at which a large number of different configurations can be found at the interface), and hence, averaged potential drops.

(iii) The IDIS model assumes that the potential drop is entirely driven by charge-transfer processes, in contrast to the results presented in the previous subsection on C_{60}/pentacene, which show that only polarization effects are responsible for the interface dipole.

(iv) The screening factor in the IDIS model is expressed in terms of the dielectric constants characteristic of the bulk phases; in fact, if charge-transfer states were present, they would actually be expected to be much less screened because the charges would be lying on adjacent molecules.[118]

Alternatively, the electronic structure of a model donor–acceptor interface can be assessed at a full quantum-chemical level. An interesting reference system is the interface between TTF as donor and TCNQ as acceptor (see the chemical structures in Figure 10), for which a potential drop of 0.6 eV has been reported from UPS measurements.[119] DFT calculations have been performed on model TTF/TCNQ complexes using the BH&HLYP functional (which includes 50% of HF exchange) that was found to provide a good description of charge transfer states by implicitly taking into account medium effects.[120]

Figure 10A illustrates the evolution of the dipole moment along the (Z-axis) stacking direction (which is the direction that matters in terms of potential drop at the interface), as a function of the intermolecular separation between the molecules in a TTF/TCNQ cofacial complex.[120] As intuitively expected, the results show a decrease in dipole moment with intermolecular distance. However, the dipole moment is made of two distinct components that evolve in different ways: (i) the dipole component calculated from the ground-state charge transfer between the molecules drops with increasing distance based on Coulomb's law and quickly reaches a vanishingly small value beyond 5 Å because of poor orbital overlap; (ii) the remaining long-range contribution is associated to polarization effects that can be seen as a longitudinal polarization of the p_z atomic orbitals of the individual atoms in the complex. Figure 10B illustrates the evolution of the Z-component of the dipole in a TTF/TCNQ dimer when translating one molecule along the Y axis for a fixed intermolecular distance of 3.5 Å. This points to the high sensitivity of the dipole moment with respect to the relative positions of the two interacting molecules; this evolution can be fully rationalized from the shape of the orbitals by estimating the amount of bonding versus antibonding interactions in the overlapping region for each specific configuration.[116] Note also that the dipole moments calculated in bimolecular complexes such as those considered in refs 121 and 122 are likely to be reduced at interfaces as a result of depolarization effects (that come from charge redistributions due to interactions among the individual molecular dipoles).

Thus, the quantum-chemical calculations indicate that the interfacial potential drops measured by UPS have to be seen as average values, while significant distributions of dipole values are expected at the nanoscale, as discussed above. Moreover, the results show that the alignment of the electronic levels at the interface is strongly modified by charge-transfer effects; in the case of the TTF/TCNQ complex, the ground-state charge transfer from donor to acceptor yields a stabilization of the TTF frontier electronic levels by a few tenths of an eV and a destabilization of the TCNQ frontier levels by the same amount. On the basis of these results, applying eq 1 to the TTF-TCNQ interface would lead to a VLS value on the order of 0.75 eV, which is in reasonable agreement with the experimental value of 0.6 eV.[123] Such interfacial electronic processes thus strongly perturb the energy diagrams that are based on the ionization potentials and electron affinities of the isolated materials, which should impact the performance of organic light-emitting
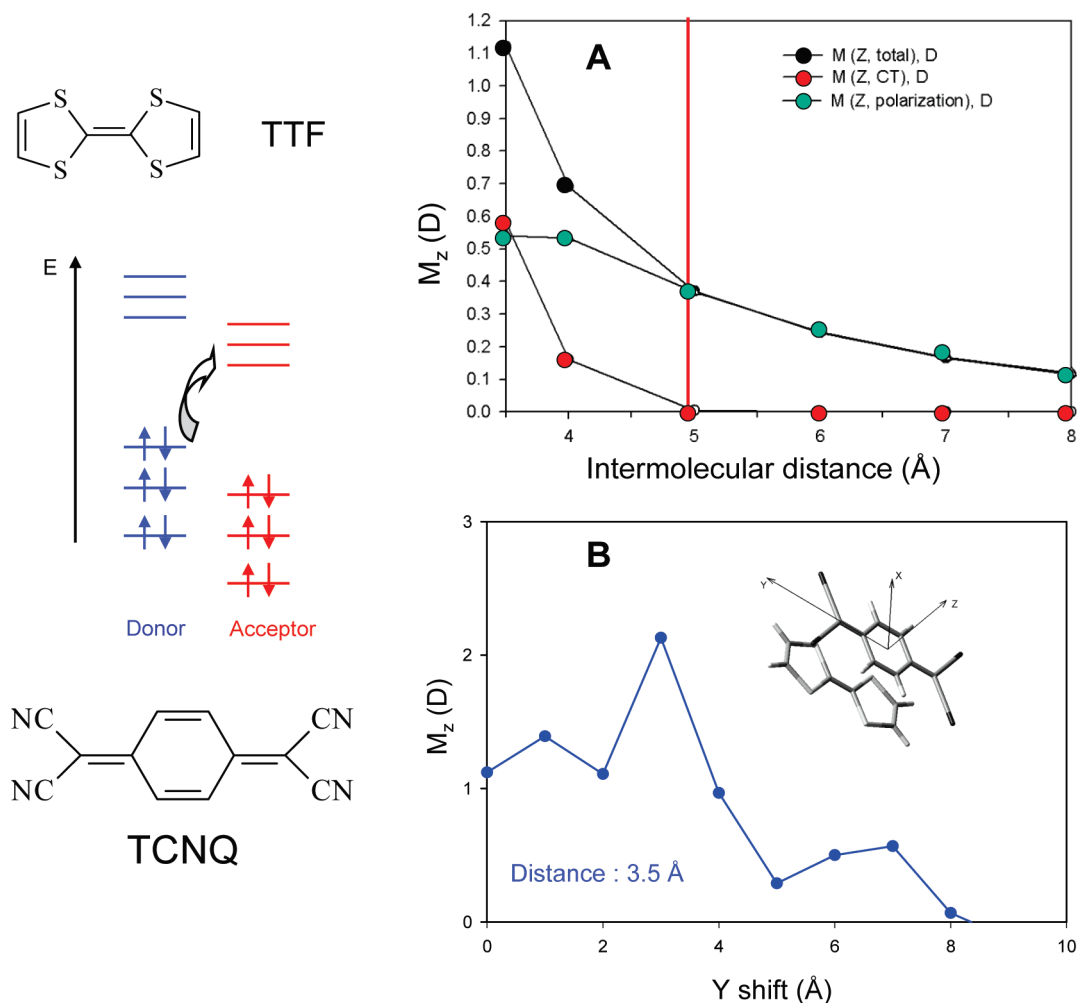
Figure 10. (A) Evolution of the component of the total dipole moment normal to the molecular planes (black circles) and of the charge-transfer contribution from Mulliken charges (red circles) in a cofacial TTF/TCNQ dimer as a function of the intermolecular distance. The curve with green circles shows the polarization component of the dipole. (B) Evolution of the component of the total dipole moment normal to the molecular planes in the TTF/TNCQ dimer as a function of the lateral shift between the molecular centers, for a fixed distance of 3.5 Å. We also display on the left side the chemical structures of TTF and TCNQ as well as the illustration of a charge-transfer excitation from D to A. Adapted with permission from ref 120. Copyright 2009 Wiley.

diodes and solar cells. In OPVs, it is likely that interfacial dipoles will affect both the driving force for charge separation (vide supra) and the open-circuit voltage (V_{oc}) that is related to the energy difference between the ionization potential of the donor and the electron affinity of the acceptor (vide infra[19]).

We note that when the two molecules interact only very weakly, due for instance to their separation by alkyl side-chains, no partial charge transfer is expected because of the absence of orbital overlap. However, in such an instance, full charge transfer could occur via tunneling across the insulating barrier if the resulting charge-transfer state is more stable than the neutral ground state.[124]

4. Modeling the Excited-State Electronic Structure at O:O Interfaces

Diabatic States and Marcus Rates. The previous sections discussed the alignment of the electronic levels at interfaces and pointed to the role played by charge-transfer and polarization effects. Understanding the dynamics of electron-transfer processes is also of utmost importance to understand the efficiency of devices at the

molecular level and to define new strategies to enhance their performance. In the case of solar cells, electron transfer from the excited donor [acceptor] to the neutral acceptor [donor] should be faster than any internal decay process to ensure a high efficiency of charge generation. Moreover, the rate of charge separation into free carriers should be larger than the recombination rate from the charge-transfer state to the ground state or a triplet excited state.[125]

Because all these events involve an electron transfer, the rate of such reactions can be estimated at the theoretical level using Marcus theory and its extensions. In the simplest form (i.e., in the semiclassical limit, which implies that the vibrational modes are treated classically), the Marcus expression is written as[126,127]

$$k = \left(\frac{4\pi^2}{h}\right) V_{if}^2 \left(\frac{1}{\sqrt{4\pi\lambda kT}}\right) \exp\left(\frac{-(\Delta G^\circ + \lambda)^2}{4\lambda kT}\right) \quad (3)$$

where V_{if} denotes the electronic coupling between the initial and final states, λ the total reorganization energy associated to the charge transfer process, ΔG° the free
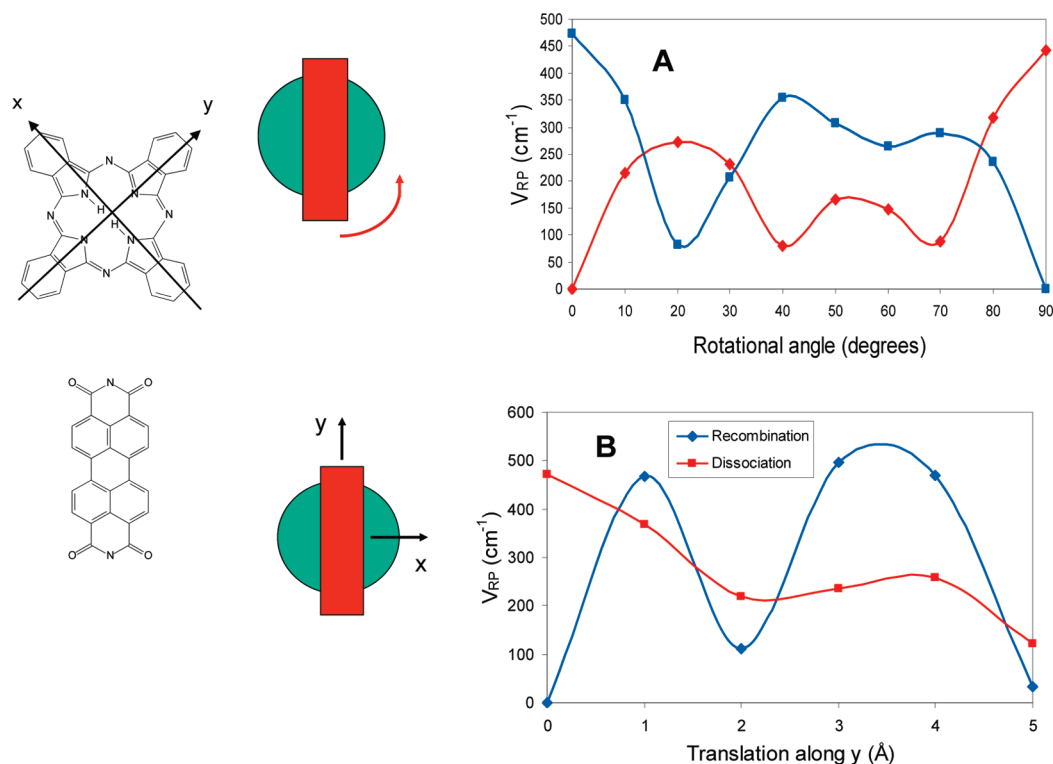
Figure 11. Evolution of the INDO/SCI-calculated electronic coupling of: (A) the two dissociation pathways in the Pc/PTCDI complex when rotating PTCDI on top of PC; (B) one pathway for exciton dissociation and charge recombination when translating the PTCDI molecule along the *y* axis. The intermolecular distance has been fixed at 5 Å. We also display the chemical structures of the two compounds. Adapted with permission from ref 115. Copyright 2005 American Chemical Society.

enthalpy of the reaction, T the temperature, and k the Boltzmann constant. The origin of the first three parameters and the way they can be estimated at the theoretical level are described in the next paragraphs.

Note that expressions accounting for tunneling effects across the barrier have also been derived. This framework has been widely used to investigate excited-state dynamics in D/A dyads in solution.[128] Before presenting a discussion of the different parameters entering the rate expression, it is worth stressing that eq 3 is obtained from perturbation theory and assumes weak coupling between donor and acceptor. Thus, the reactant and product states in the Marcus picture are based on the diabatic potential energy curves in the initial and final states (for instance, $|D^*A\rangle$ and $|D^+A^-\rangle$ in the case of photoinduced electron transfer from the optically excited donor). We will describe the nature of the adiabatic states and their dynamics at the end of this Section. There are three parameters in eq 3, which we now address in turn.

V_{if} represents the electronic coupling between the initial and final states. It reflects the ease of electron exchange between the two molecules. When the relevant states can be described in a one-electron picture (for instance, $|D^*A\rangle$ by a HOMO-to-LUMO transition in the donor; $|DA^*\rangle$ by a HOMO-to-LUMO transition in the acceptor; and $|D^+A^-\rangle$ by an excitation from one occupied level of D to one unoccupied level of A) and when the population of a single molecular orbital is changed upon electron transfer, V_{if} corresponds to the transfer integral between the orbitals involved in the process (for instance, between

$LUMO_D$ and $LUMO_A$ for $|D^*A\rangle \rightarrow |D^+A^-\rangle$, $HOMO_D$ and $HOMO_A$ for $|DA^*\rangle \rightarrow |D^+A^-\rangle$, or $HOMO_D$ and $LUMO_A$ for $|D^+A^-\rangle \rightarrow |DA\rangle$). Such transfer integrals can be directly computed at various levels of theory.[129,130]

The amplitude of the electronic coupling is a function of the relative positions of the interacting molecules. For the sake of illustration, Figure 11A collects the electronic couplings (computed at the semiempirical INDO level) for exciton dissociation $|DA^*\rangle \rightarrow |D^+A^-\rangle$ from the two quasi-degenerate LUMO orbitals of metal-free phthalocyanine (Pc) to the LUMO of perylenetetracarboxydiimide (PTCDI), as a function of the rotation of PTCDI on top of Pc (the intermolecular distance being fixed at 4 Å).[113] The LUMOs of Pc are extended along one branch of the molecule (along either the *X* or *Y* axis) and have different symmetries. When the PTCDI molecule is initially positioned on top of one Pc branch in a symmetric cofacial fashion, symmetry rules make one $LUMO_{PC} \rightarrow LUMO_{PTCDI}$ transition forbidden (the amount of bonding character in the overlapping region exactly cancels the amount of antibonding interactions[115]) while the other is active, as shown in Figure 11A. When PTCDI is rotated by 90°, the forbidden channel becomes active and vice versa, once again because of symmetry effects intimately linked to the shape of the molecular orbitals.[131] For intermediate rotational angles, both channels are found to be efficient, which highlights the interest of two- or three-dimensional systems that can give rise to multiple pathways for photoinduced charge generation. Figure 11B illustrates the evolution of the electronic couplings associated

to one dissociation channel and the recombination channel ($|D^+A^-\rangle \rightarrow |DA\rangle$) when translating PTCDI along the Y-axis. The electronic coupling for recombination is strictly zero in the initial cofacial geometry; however, electronic couplings for recombination larger than for dissociation are calculated when breaking the symmetry constraints upon translation of the PTCDI molecule. Lattice dynamics is also expected to modulate the amplitude of the transfer integrals.[42,132] As briefly mentioned earlier, similar calculations recently performed on C_{60}/pentacene complexes have shown that the rate of charge recombination is much faster when C_{60} is lying on top of a flat-lying pentacene molecule, compared to a geometry where C_{60} is positioned at the edge of pentacene;[52] the efficiency of the recombination pathway going from the lowest CT state to the lowest triplet excited state of pentacene has also been evidenced.[52] These calculations have recently been extended to a comparison of the exciton-dissociation and charge-recombination rates in oligothiophene/C_{60} and oligothiophene/PTCDI complexes.[133]

Note that so far we have implicitly assumed here that exciton dissociation occurs from the lowest excited state directly down to the lowest charge-transfer state. However, pathways along which the local excitation first decays into a higher-lying CT state (involving different molecular orbitals) are likely to play a significant role in helping either to reach the lowest CT state (by reducing the energy gap between the initial and final states involved in the electron-transfer process) or to dissociate the CT pair from such a "hot" state.[23,134] This is in essence the "hot-state"-mediated charge generation pathway referred to in section III and ref 87 In this respect, quantum-chemical calculations performed on model systems have shown that the electronic coupling to higher-lying CT states can indeed be sometimes larger compared to the lowest CT state due to symmetry effects.[52,133,134]

A second parameter in eq 3 is λ, the total reorganization energy, which is made of an internal and an external component. Since the geometry of conjugated molecules is markedly different in the ground, charged, and excited states due their strong electron-vibration couplings, the internal part reflects the amount of geometric relaxations required to evolve from the initial to the final state. The internal reorganization energy typically varies between 50 and 500 meV and can be evaluated routinely from first-principles calculations.[129] The external part represents the changes in electronic polarizations within the surrounding molecules following electron transfer and their geometric reorganizations. The external reorganization energy is far from being trivial to estimate and can be evaluated to a very first approximation from a continuum model developed by Marcus and co-workers for spherical ions in solution, with the parameters adjusted to organic semiconductors in the bulk.[115] More elegant approaches based on hybrid QM/MM approaches[135,136] or quantum sampling of vibrations coupled to quantum-chemical calculations[137] have led to values ranging from a few millielectronvolts up to 50 meV in molecular crystals.

The third parameter, $\Delta G°$, is the Gibbs free energy of the reaction. When neglecting entropy effects, it represents the energy difference between the initial and final states. In a simple one-electron picture, $\Delta G°$ in the case of, for instance, the $|DA^*\rangle \rightarrow |D^+A^-\rangle$ process would correspond to the energy difference between the LUMO levels of the D and A molecules at the interface plus the Coulomb attraction within the generated charge pair. This energy difference will also be affected by any electronic interactions at the interface, as discussed in the previous sections. Note that in Marcus theory the largest electron-transfer rates are obtained when the energy gain between initial and final states upon exothermic charge transfer is exactly compensated by the reorganization energy.

Estimating the energy of a charge-transfer state within a polarizable medium is a challenging task at the quantum-chemical level. A simple approach used in previous studies consists in estimating the total energy of the individual species (D^*, A, D^+, A^-) by using a continuum solvation model and in computing the Coulomb term from the calculated atomic charges, with a dielectric screening characteristic of organic media (around 3−4).[115] That this approach provides realistic values of $\Delta G°$[138] actually comes from a compensation of errors. Indeed, the polarization energy of the isolated D^+ and A^- units is larger than the polarization energy of the globally neutral D^+A^- pair;[49] on the other hand, using the dielectric constant of the bulk medium underestimates the Coulomb term because the charges are actually sitting on adjacent molecules. Being able to estimate the exact energy of the CT states is also of high importance for solar cells because equivalent-circuit models (developed from semiconductor physics) indicate that the open-circuit voltage is limited by thermal excitations from the ground state to the lowest CT state.[139]

Plugging all three parameters into the Marcus rate expression yields the electron-transfer rates for the key electronic processes in solar cells or light-emitting diodes. In the case of PTCDI/Pc or pentacene/C_{60} complexes used for solar cells,[42,114] the recombination rates to the ground state are generally slower than the exciton-dissociation rate due to the fact that the former process generally takes place within the inverted region of Marcus theory (i.e., $|\Delta G°| \gg \lambda$). However, in many instances, the recombination rates are lower by only two or 3 orders of magnitude, indicating that it can compete with the rate of generation of free carriers. Again, we emphasize that the relative time scales for charge-recombination and exciton-dissociation processes strongly depend on the geometric configurations at the interfaces (through the V_{if} factor above), with face-to-face structures generally leading to more efficient nonradiative decay to the ground state than side-by-side structures.[52,133]

Excited-State Charge Transfer and Exciplexes. In addition to the description of ground-state electronic interactions, Mulliken charge transfer theory can easily be generalized to account for excited-state electronic interactions.[140] This can be done by including in the basis set the lowest diabatic electronic excited states of the donor and acceptor molecules $|D^*A\rangle$, $|DA^*\rangle$; as will be shown below, this approach is particularly relevant to the case of moderate energy mismatch between the electronic structure

of the donor and the acceptor (namely for heterojunctions designed to produce large V_{OC} OPV cells). The combination of localized covalent electronic excitations and ionic charge-transfer configurations then yields an excited state with mixed covalent-ionic character, referred to as an exciplex state, $|\Psi_{XP}\rangle$

$$|\psi_{XP}\rangle = a|D^+A^-\rangle + a'|D^-A^+\rangle$$
$$+ b|DA\rangle + c|D^*A\rangle + c'|DA^*\rangle \qquad (4)$$

It is clear from eq 4 that exciplexes can span the whole range of ionicity from purely charge separated states (b,c, $c' \approx 0$) to purely covalent localized excited states (a,a', $b \approx 0$). In both limiting cases, the diabatic description presented above prevails. Because the energy separation among diabatic excited configurations is usually smaller than their energy difference to the ground state (and since, in a perturbative scheme, the amount of mixing scales with the inverse energy separation), $b \ll a,a',c,c'$ so that exciplex formation is not necessarily accompanied by substantial ground-state interactions. Rather, exciplexes (or, in the case where the interacting molecules are the same (i.e., D = A), excimers) have a repulsive ground state and are mostly stabilized by resonance interactions between localized covalent and charge-transfer ionic configurations in the excited state. The resulting admixture of charge-transfer character into the lowest electronic excited state usually entails strong couplings to intermolecular vibrational modes that bring D and A closer to one another in the relaxed geometric configuration; this results in red-shifted, broad, and featureless emission spectra.[141]

We now briefly review some experimental and theoretical works underlining the importance of such interfacial excited states in the photophysics of blended or multilayer films based on conjugated molecules and polymers. Note that in doing this we extend our discussion to both light-emitting diodes and photovoltaic cells, as it turns out that such mixed-character electronic states can act as precursors for either light emission or charge recombination.

Using time-resolved fluorescence and photoinduced absorption spectroscopy, Jenekhe and Osaheni have shown that the low photoluminescence quantum yields measured for various acceptor conjugated polymers in the presence of tris(*p*-tolyl)amine as donor, can be ascribed to the formation of exciplexes.[142] Similar experiments have been reported for blends of two semiconducting polymers that demonstrated the formation of luminescent exciplexes at the interfaces between the two materials.[125] Exciplexes can be used as emission sources in light-emitting diodes, as demonstrated, e.g., for bilayers of diamine and either quinoxaline[143] or silole derivatives.[144] In the latter case, an electroluminescence quantum yield of 3.4% was achieved at 100 A/m².[144] Exciplex emission in bilayer heterojunctions has also been successfully exploited in LEDs based on conjugated polymers such as poly(pyridylvinylene-phenylenevinylene).[145] When the two layers are prepared by blending green-emitting copolymers into different polyfluorenes, LEDs with efficient

white light emission have been demonstrated.[146] Sometimes, excimers and exciplexes are only observed upon electrical excitation, i.e., by charge recombination in a LED, and not upon optical excitation. In this case, they are referred to as electromers or electroplexes. Though little is known about their formation pathway, it is notable that electroplexes and exciplexes are generally reported in the case of materials that contain a nitrogen atom in certain moieties. For example, electroplexes are known for combinations of organic semiconductors that contain carbazole, amine, oxadiazole, and other diazole moieties.[147−154]

The radiative decay of these exciplexes (or electroplexes) to the ground state becomes allowed as a result of the (small) admixture of covalent localized electronic excitations into their wave functions, as described in eq 4. This has been quantified in refs 155,156 for blends between either poly(9,9-dioctylfluorene-co-bis-*N,N*-(4-butylphenyl)-bis-*N,N*-phenyl-1,4-phenylenediamine) (PFB) or poly-(9,9-dioctylfluorene-co-*N*-(4-butylphenyl) diphenyl-amine) (TFB) as donor and poly(9,9-dioctylfluorene-co-benzothiadiazole) (F8BT) as acceptor. Sreearunothai et al. have shown that different orientations of the molecules at the heterojunction result in either repulsive or attractive interchain interactions.[156] Calculations of the Coulomb interaction between excitonic excited states on one chain and the ground state on the other revealed that although repulsive interactions lead to a blue-shifted exciton emission, attractive interactions favor the formation of exciplex states. This highlights the need for a quantitative description of the dispersion and electrostatic forces driving the supermolecular arrangements of conjugated molecules/polymer chains in the solid state, as pointed out above.

By expanding $|\Psi_{XP}\rangle$ in a molecular orbital basis and assuming for simplicity a three-orbital model (i.e., the charge-transfer excitation corresponds to $|H_{PFB} \rightarrow L_{F8BT}\rangle$ and the localized excitation on the acceptor is $|H_{F8BT} \rightarrow L_{F8BT}\rangle$, where H_{PFB}, H_{F8BT}, and L_{F8BT} denote the HOMOs of PFB and F8BT and the LUMO of F8BT, respectively), the overall transition dipole moment to the lowest excited state in the complex can be recast from first-order perturbation theory as (neglecting ground-state interactions and the higher-lying donor excited states)

$$\langle\psi_{GS}|\mu|\psi_{XP}\rangle = c_{CT}\langle H_{PFB}|\mu|L_{F8BT}\rangle$$

$$+ c_{EX}\langle H_{F8BT}|\mu|L_{F8BT}\rangle \approx c_{CT}\langle H_{PFB}|\mu|L_{F8BT}\rangle$$

$$+ \frac{\langle H_{PFB}|t|H_{F8BT}\rangle}{E_{EX} - E_{CT}}\langle H_{F8BT}|\mu|L_{F8BT}\rangle \qquad (5)$$

where E_{EX} and E_{CT} denote the energies of pure local and charge-transfer electronic configurations, respectively, and $\langle H_{PFB}|t|H_{F8BT}\rangle$ is the (one-electron) matrix element mixing the HOMOs of the PFB and F8BT chains and $c_{CT} \leq 1$. Therefore, the exciplex states acquire absorption cross sections and finite radiative lifetimes through either
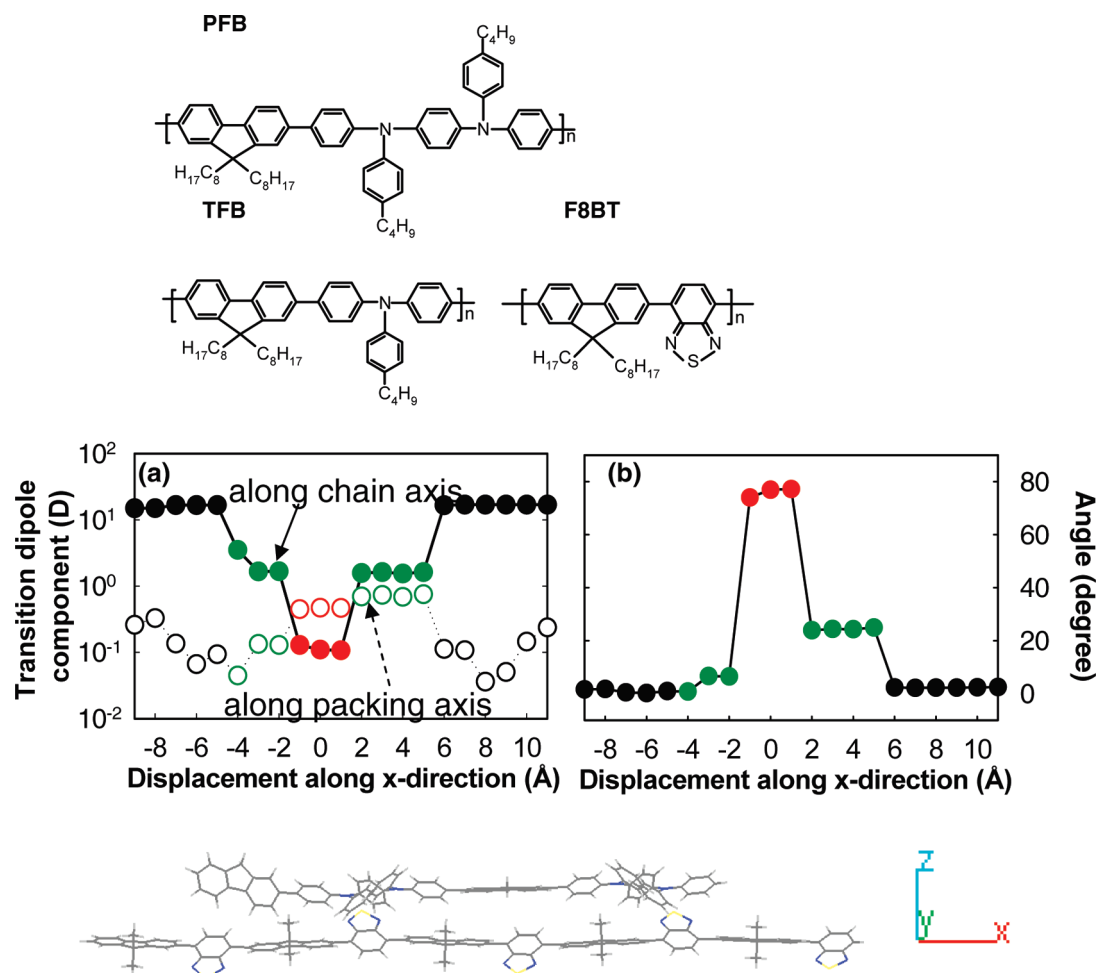
Figure 12. (a)Transition dipole moment to the lowest electronic excited state of a PFB:F8BT donor:acceptor interface and (b) rotation angle, θ, between the transition dipole moment and the chain axis as a function of longitudinal displacements of the polymer chains. The different colors refer to the different nature of the electronic excitation: exciton (black), exciplex (green), and charge transfer or polaron pair (red). Adapted with permission from ref 155. Copyright 2008 Nature Publishing Group.

direct overlap between the HOMO and LUMO of the interacting molecules (first term in eq 5) or mixing with the F8BT localized excitation (second term in eq 5).

It is interesting to consider the polarization of the two contributions in eq 5: while the direct overlap term contributes a transition dipole moment component along the stacking axis (Z-axis here), the interaction between local and charge-transfer configurations provides an XY-polarized component resulting from intensity borrowing from the F8BT excitonic transition. In Figure 12a, the INDO/SCI average values of the transition dipole components along the stacking axis and in the perpendicular molecular planes are shown for representative configurations obtained by displacing one chain with respect to the other.[155] It is seen that the transition dipole moment to the exciplex states arises primarily from the mixing between charge-transfer (polaron pair) and excitonic configurations, i.e., it is mostly polarized in the XY-plane (the second term in eq 5 dominates). In contrast, pure polaron-pair configurations show transition dipole moments that are smaller and oriented along the stacking axis, as they result from direct overlap between the HOMO orbital of PFB and the LUMO orbital of F8BT. The angle θ between the transition dipole moment and the chain-axis direction

is smaller than 3° for the excitonic states, close to 75° for polaron-pair states, and intermediate for exciplexes (Figure 12b). These theoretical results are consistent with experimental values coming from luminescence depolarization measurements that indicate an angle θ of about 45° for exciplex emission, which suggests that exciplexes have a significant transition dipole moment perpendicular to the excitonic (in-chain) direction.[155]

Besides direct radiative recombination, exciplexes can also mediate light emission in LEDs via an endothermic energy transfer to the bulk highly emissive excitons.[100,157] Thus, electrical excitation generates charge carriers that are stored as exciplexes or pure polaron pairs and subsequently up-convert to produce light. This process requires low charge densities at the interface and a small energy mismatch between the exciplexes and the bulk excitons for efficient uphill energy conversion. It is also important to stress that exciplexes, in contrast to excitons, are localized and rather immobile, so that the local electronic properties of the heterojunction states become crucial for the overall device performance.

As described previously, interfacial excited states can span the whole range of ionicity from pure excitons to pure charge-transfer states, depending on the nature of
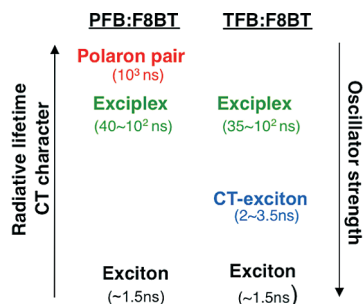
Figure 13. Schematic of the lowest electronic excitations at the PFB: F8BT and TFB:F8BT interfaces. Reproduced with permission from ref 155. Copyright 2008 Nature Publishing Group.

the interacting donor and acceptor units as well as on their relative orientations and distances. This is illustrated in Figure 13 that shows the wide range of interfacial electronic states identified from quantum-chemical calculations on PFB:F8BT and TFB:F8BT blends. One might anticipate that electronic states with predominant charge-transfer character could act as intermediates for efficient photoinduced charge generation in photovoltaic cells; however, the caveat is that these are strongly Coulomb-bound charge pairs.

In addition to the field-assisted charge generation process discussed in Section III, another scenario has also been proposed according to which the thermally "hot" CT-like states generated from the early photoinduced charge-separation process use their excess thermal energy to compensate for the Coulomb attraction between the charges. Obviously, this requires that charge generation occurs from an "excited" charge-transfer state on a time scale shorter than thermal relaxation. The formation of hot CT excitons corresponding to solutions of the atomic H-like Schrödinger equation with different values of the principal and angular momentum quantum numbers has been demonstrated from two-photon photoemission spectra at the model pentacene:vacuum interface;[158] however, their role in charge dissociation remains elusive.[87] In addition, in the case where the lower-lying electronic excitations are localized triplet excitons, these can act as sinks for the photoconversion because of fast intersystem crossing from the singlet to the triplet manifold in the CT excited state followed by internal conversion. This turns out to be the case in material combinations with small energy offsets between the HOMO and LUMO levels (leading to large open-circuit voltages) such as blends of polyfluorenes with F8BT.[159] There, it is found that the photogenerated charge pairs are remarkably immobile at the heterojunction during their lifetime; the charge pairs are subject to efficient intersystem crossing and 75% of them eventually recombine into F8BT triplet excitons, thereby contributing to a major loss mechanism for the PV cells.[159]

The dynamics of charge generation in polymer blends has been elegantly modeled by Bittner and co-workers who applied either a time-convolutionless master equation or the numerically exact multiconfigurational time-dependent Hartree method to solve an electron–phonon model.[160−162] In the case of TFB:F8BT blends, these authors showed that the efficiency of exciton dissociation critically depends on the presence of intermediate (hot) CT states as well as on the dynamical interplay of high- and low-frequency phonon modes. The ultrafast, highly nonequilibrium dynamics, was found to be consistent with the experimental finding that exciton decay to free-charge carriers and recombination phenomena compete at TFB:F8BT interfaces.

V. Conclusions and Perspectives

This short review has highlighted that the description of the discontinuity in geometric and electronic structure at organic/organic donor/acceptor interfaces remains a formidable challenge:

Indeed, the simulation of the morphology of O:O interfaces requires the synergistic application of tools from soft matter physics, crystallography, and crystal growth science to systems with large sizes (at least a few nanometers, which corresponds to thousands of atoms) and for long time scales (often hundreds of nanoseconds). In addition, these structural calculations need to keep track of the atomistic details for subsequent quantum-mechanical calculations.

The electronic structure at O:O interfaces results from a subtle balance between a number of effects that are usually difficult to address using conventional quantum-chemical or solid-state physics theory, namely ground-state intermolecular charge transfer, electronic polarization effects induced by excess charges, or electronic excited states described by a mixing between charge-transfer and local configurations. Moreover, these effects are extremely sensitive to the relative distances and orientations of the donor and acceptor molecules at the interface.

The evolutions of the primary electronic excitations generated in OPVs or OLEDs depend not only on the energetics at the interface, but also on the relative time scales of competing processes corresponding to exciton dissociation, charge separation, and charge recombination into the ground state or triplet excited states. The energy diagrams for these processes need to be built by taking fully into account the interfacial effects; an increasing number of experimental and theoretical data point to the existence of a vacuum-level shift associated to an interfacial dipole, that originates from ground-state (partial) charge transfer and/or electronic polarization effects.

The results we have reviewed illustrate some of the first attempts toward a systematic study of the relationships between the chemical structure of the donor and acceptor molecules, their relative orientations in blends or multi-layer architectures, the impact on the electronic structure at the interfaces, and the implications for the energetics and dynamics of electronic excited states in opto-electronic devices. Clearly, the picture is far from being complete and will ultimately require the development and implementation, within the same framework, of theoretical methods combining large-scale simulations of interface

morphology, correlated ab initio calculations of the interfacial electronic structure in the ground and excited states, and quantum-dynamics simulations following the evolution of the relevant electronic states coupled to the vibrational bath over many orders of magnitude in time.

References

(1) Kepler, R. G.; Bierstedt, P. E.; Merrifield, R. E. *Phys. Rev. Lett.* **1960**, *5*, 503.

(2) Melby, L. R.; Harder, R. J.; Hertler, W. R.; Mahler, W.; Benson, R. E.; Mochel, W. E. *J. Am. Chem. Soc.* **1962**, *84*, 3374.

(3) Epstein, A. J.; Etemad, S.; Garito, A. F.; Heeger, A. J. *Phys. Rev. B* **1972**, *5*, 952.

(4) See, for instance, the special issue on "Molecular Conductors", guest edited by Batail, P. Chem. Rev. **2004**, *104*, 4887−5781.

(5) Ferraris, J.; Cowan, D. O.; Walatka, V.; Perlstein, J. H. *J. Am. Chem. Soc.* **1973**, *95*, 948.

(6) Coleman, L. B.; Cohen, M. J.; Sandman, D. J.; Yamagishi, F. G.; Garito, A. F.; Heeger, A. J. *Solid State Commun.* **1973**, *12*, 1125.

(7) Jérôme, D.; Mazaud, M.; Ribault, M.; Bechgaard, K. *J. Phys. Lett.* **1980**, *41*, L95.

(8) Tanaka, H.; Okano, Y.; Kobayashi, H.; Suzuki, W.; Kobayashi, A. *Science* **2001**, *291*, 285.

(9) Shirakawa, H.; Louis, E. J.; MacDiarmid, A. G.; Chiang, C. K.; Heeger, A. J. *Chem. Commun.* **1977**, 578.

(10) Basescu, N.; Liu, Z. X.; Moses, D.; Heeger, A. J.; Naarmann, H.; Theophilou, N. *Nature (London)* **1987**, *327*, 403.

(11) See, for instance: *Handbook of Conducting Polymers: Theory, Synthesis, Properties, and Characterization*, third ed.; Skotheim, T.A., Reynolds, J.R., Eds.; CRC Press: Boca Raton, FL, 2007.

(12) See, for instance: *Handbook of Conducting Polymers: Processing and Applications*, third ed.; Skotheim, T.A., Reynolds, J.R., Eds.; CRC Press, Boca Raton, FL, 2007.

(13) Tang, C. W.; Van Slyke, S. A. *Appl. Phys. Lett.* **1987**, *51*, 913.

(14) Burroughes, J. H.; Bradley, D. D. C.; Brown, A. R.; Marks, R. N.; MacKay, K.; Friend, R. H.; Burns, P. L.; Holmes, A. B. *Nature* **1990**, *347*, 539.

(15) Friend, R. H.; Gymer, R. W.; Holmes, A. B.; Burroughes, J. H.; Marks, R. N.; Taliani, C.; Bradley, D. D. C.; dos Santos, D. A.; Brédas, J. L.; Lögdlund, M.; Salaneck, W. R. *Nature* **1999**, *397*, 121.

(16) Garnier, F.; Hajlaoui, R.; Yassar, A.; Srivastava, P. *Science* **1994**, *265*, 1684.

(17) Tang, C. W. *Appl. Phys. Lett.* **1986**, *48*, 183.

(18) Walzer, K.; Maennig, B.; Pfeiffer, M.; Leo, K. *Chem. Rev.* **2007**, *107*, 1233.

(19) Vandewal, K.; Tvingstedt, K.; Gadisa, A.; Inganäs, O.; Manca, J. V. *Nat. Mater.* **2009**, *8*, 904.

(20) Potscavage, W. J.; Yoo, S.; Kippelen, B. *Appl. Phys. Lett.* **2008**, *93*, 193308.

(21) Venkataraman, D.; Yurt, S.; Harihara Venkatraman, B.; Gavvalapalli, N. *J. Phys. Chem. Lett.* **2010**, *1*, 947.

(22) Perez, M. D.; Borek, C.; Forrest, S. R.; Thompson, M. E. *J. Am. Chem. Soc.* **2009**, *131*, 9281.

(23) See, for instance, the special issue on "Organic Photovoltaics", guest edited by Brédas, J. L.; Durrant, J.D. Acc. Chem. Res. **2009**, *42*, 1689−1857.

(24) Brédas, J. L.; Norton, J. E.; Cornil, J.; Coropceanu, V. *Acc. Chem. Res.* **2009**, *42*, 1691.

(25) Dunitz, J. D.; Gavezzotti, A. *Chem. Soc. Rev.* **2009**, *38*, 2622.

(26) Rice, S. L. *Acc. Chem. Res.* **2009**, *42*, 117.

(27) Cheng, H.-L.; Mai, Y.-S.; Chou, W.-Y.; Chang, L.-R.; Liang, X.-W. *Adv. Funct. Mater.* **2007**, *17*, 3639.

(28) Della Valle, R. G.; Brillante, A.; Venuti, E.; Farina, L.; Girlando, A.; Masino, M. *Org. Electron.* **2004**, *5*, 1.

(29) Chen, L.-M.; Hong, Z.; Li, G.; Yang, Y. *Adv. Mater.* **2009**, *21*, 1434.

(30) Hooks, D. E.; Fritz, T.; Ward, M. D. *Adv. Mater.* **2001**, *13*, 227.

(31) Mannsfeld, S. C. B.; Fritz, T. *Mod. Phys. Lett. B* **2006**, *20*, 585.

(32) Yamamoto, T. *Polymer* **2009**, *50*, 1975.

(33) Misbah, C.; Pierre-Louis, O.; Saito, Y. *Rev. Modern. Phys.* **2010**, *82*, 981.

(34) Choudhary, D.; Clancy, P.; Shetty, R.; Escobedo, F. *Adv. Funct. Mater.* **2006**, *16*, 1768.

(35) Liu, H.; Lin, Z.; Zhigilei, L. V.; Reinke, P. *J. Phys. Chem. C* **2008**, *112*, 4687.

(36) Frenkel, D.; Smit, B. *Understanding Molecular Simulation−From Algorithms to Applications*; Academic Press: New York, 2002.

(37) Leach, A. R. *Molecular Modeling: Principles and Applications*; Prentice Hall: Upper Saddle River, NJ, 2001.

(38) Kratzer, P. Monte Carlo and Kinetic Monte Carlo Methods−A Tutorial. In *Multiscale Simulation Methods in Molecular Sciences*; Grotendorst, J., Attig, N., Blügel, S., Marx, D., Eds.; NIC Series; Institute for Advanced Simulation, Forschungszentrum Jülich: Jülich, Germany, 2009; Vol. 42, pp 51−76; http://arxiv.org/abs/0904.2556

(39) Gillespie, D. T. *Annu. Rev. Phys. Chem.* **2007**, *58*, 35.

(40) Olivier, Y.; Muccioli, L.; Lemaur, V.; Geerts, Y. H.; Zannoni, C.; Cornil, J. *J. Phys. Chem. B.* **2009**, *113*, 14102.

(41) Martinelli, N. G.; Savini, M.; Muccioli, L.; Olivier, Y.; Castet, F.; Zannoni, C.; Beljonne, D.; Cornil, J. *Adv. Funct. Mater.* **2009**, *19*, 3254.

(42) Martinelli, N. G.; Olivier, Y.; Athanasopoulos, S.; Delgado, M. C. R.; Pigg, K. R.; da Silva, D. A.; Sanchez-Carrera, R. S.; Venuti, E.; Della Valle, R. G.; Brédas, J.-L.; Beljonne, D.; Cornil, J. *ChemPhysChem* **2009**, *10*, 2265.

(43) Piana, S.; Gale, J. D. *J. Cryst. Growth* **2006**, *294*, 46.

(44) Peumans, P.; Uchida, S.; Forrest, S. R. *Nature* **2003**, *425*, 158.

(45) Orlandi, S.; Muccioli, L.; Ricci, M.; Zannoni, C. *Soft Matter* **2009**, *5*, 4484.

(46) Karayiannis, N. C.; Martin Kröger, M. *Int. J. Mol. Sci.* **2009**, *10*, 5054.

(47) Campione, M.; Raimondo, L.; Moret, M.; Campiglio, P.; Fumagalli, E.; Sassella, A. *Chem. Mater.* **2009**, *21*, 4859.

(48) Campione, M.; Moret, M.; Raimondo, L.; Sassella, A. *J. Phys. Chem. C* **2009**, *113*, 20927.

(49) Verlaak, S.; Beljonne, D.; Cheyns, D.; Rolin, C.; Linares, M.; Castet, F.; Cornil, J.; Heremans, P. *Adv. Funct. Mater.* **2009**, *19*, 3809.

(50) Mizuseki, H.; Igarashi, N.; Belosludov, R. V.; Farajian, A. A.; Kawazoe, Y. *Synth. Met.* **2003**, *138*, 281.

(51) Tamura, H.; Ramon, J. G. S.; Bittner, E. R.; Burghardt, I. *J. Phys. Chem. B* **2008**, *112*, 495.

(52) Yi, Y.; Coropceanu, V.; Brédas, J.-L. *J. Am. Chem. Soc.* **2009**, *131*, 15777.

(53) Kodama, Y.; Ohnoa, K. *Appl. Phys. Lett.* **2010**, *96*, 034101.

(54) Castet, F.; Aurel, P.; Fritsch, A.; Ducasse, L.; Liotard, D.; Linares, M.; Cornil, J.; Beljonne, D. *Phys. Rev. B* **2008**, *77*, 115210.

(55) Linares, M.; Beljonne, D.; Cornil, J.; Lancaster, K.; Brédas, J. L.; Verlaak, S.; Mityashin, A.; Heremans, P.; Fuchs, A.; Lennartz, C.; Idé, J.; Méreau, R.; Aurel, P.; Ducasse, L.; Castet, F. *J. Phys. Chem. C* **2010**, *114*, 3215.

(56) Peter, C.; Kremer, K. *Soft Matter* **2009**, *5*, 4357.

(57) Watkins, P. K.; Walker, A. B.; Verschoor, G. L. B. *Nano Lett.* **2005**, *5*, 1814.

(58) Frost, J. M.; Cheynis, F.; Tuladhar, S. M.; Nelson, J. *Nano Lett.* **2006**, *6*, 1674.

(59) Yang, F.; Forrest, S. R. *ACS Nano* **2008**, *2*, 1022.

(60) Groves, C.; Koster, L. J. A.; Greenham, N. C. *J. Appl. Phys.* **2009**, *105*, 094510.

(61) Deibel, C.; Strobel, T.; Dyakonov, V. *Phys. Rev. Lett.* **2009**, *103*, 036402.

(62) Meng, L.; Shang, Y.; Li, Q.; Li, Y.; Zhan, X.; Shuai, Z.; Kimber, R. G. E.; Walker, A. B. *J. Phys. Chem. B* **2010**, *114*, 36.

(63) Kimber, R. G. E.; Walker, A. B.; Schroeder-Turkc, G. E.; Cleaver, D. J. *Phys. Chem. Chem. Phys.* **2010**, *12*, 844.

(64) Adams, C. D.; Srolovitz, D. J.; Atzmon, M. *J. Appl. Phys.* **1993**, *73*, 1707.

(65) Zannoni, C. *J. Mater. Chem.* **2001**, *11*, 2637.

(66) Micheletti, D.; Muccioli, L.; Berardi, R.; Ricci, M.; Zannoni, C. *J. Chem. Phys.* **2005**, *123*, 224705.

(67) Orlandi, S.; Muccioli, L.; Ricci, M.; Berardi, R.; Zannoni, C. *Chem. Cent. J.* **2007**, *1*, 15.

(68) Orlandi, S.; Muccioli, L.; Ricci, M.; Zannoni, C. *Soft Matter* **2009**, *5*, 4484.

(69) Bacchiocchi, C.; Hennebicq, E.; Orlandi, S.; Muccioli, L.; Beljonne, D.; Zannoni, C. *J. Phys. Chem. B* **2008**, *112*, 1752.

(70) Goto, M.; Takezoe, H.; Ishikawa, K. *J. Chem. Phys.* **2010**, *132*, 054506.

(71) Mueller-Plathe, F. *ChemPhysChem* **2002**, *3*, 754.

(72) Huang, D. M.; Faller, R.; Do, K.; Moulé, A. J. *J. Chem. Theory Comput.* **2010**, *6*, 526.

(73) Forrest, S. R.; Zhang, Y. *Phys. Rev. B* **1994**, *49*, 11297.

(74) Liu, D.-J.; Blumberg Selinger, R. L.; Weeks, J. D. *J. Chem. Phys.* **1996**, *105*, 4751.

(75) Papadopoulos, T. A.; Muccioli, L.; Athanasopoulos, S.; Walker, A. B.; Zannoni, C.; Beljonne, D., **2010**, submitted.

(76) Chang, J.; Sandler, S. I. *J. Chem. Phys.* **2006**, *125*, 054705.

(77) Marcon, V.; van der Vegt, N.; Wegner, Raos, G. *J. Phys. Chem. B* **2006**, *110*, 5253.

(78) Marcon, V.; Raos, G. *J. Am. Chem. Soc.* **2006**, *128*, 1408.

(79) Marcon, V.; Breiby, D. W.; Pisula, W.; Dahl, J.; Kirkpatrick, J.; Patwardhan, S.; Grozema, F.; Andrienko, D. *J. Am. Chem. Soc.* **2009**, *131*, 11426.

(80) Cheung, D. L.; McMahon, D. P.; Troisi, A. *J. Phys. Chem. B* **2009**, *113*, 9393.

(81) Moreno, M.; Casalegno, M.; Raos, G.; Meille, S. V.; Po, R. *J. Phys. Chem. B* **2010**, *114*, 1591.

(82) Zheng, Y.; Pregler, S. K.; Myers, J. D.; Ouyang, J.; Sinnott, S. B.; Xuea, J. *J. Vac. Sci. Technol. B* **2009**, *27*, 1071.

(83) Goose, J. E.; Clancy, P. *J. Phys. Chem. C* **2007**, *111*, 15653.

(84) Cantrell, R.; Clancy, P. *Surf. Sci.* **2008**, *602*, 3499.

(85) Goose, J. E.; First, E. L.; Clancy, P. *Phys. Rev. B* **2010**, *81*, 205310.

(86) Tiberio, G.; Muccioli, L.; Berardi, R.; Zannoni, C. *ChemPhysChem* **2009**, *10*, 125.

(87) Clarke, M. C.; Durrant, J. R. *Chem. Rev.* **2010** No. DOI:10.1021/cr900271s.

(88) Arkhipov, V. I.; Heremans, P.; Bässler, H. *Appl. Phys. Lett.* **2003**, *82*, 4605.

(89) Ishii, H.; Sugiyama, K.; Ito, E.; Seki, K. *Adv. Mater.* **1999**, *11*, 605.

(90) Veenstra, S. C.; Jonkman, H. T. *J. pol. Sci. B* **2003**, *41*, 2549.

(91) Ge, Y.; Whitten, J. E. *Chem. Phys. Lett.* **2007**, *448*, 65.

(92) Molodtsova, O. V.; Schwieger, T.; Knupfer, M. *Appl. Surf. Sci.* **2005**, *252*, 143.

(93) Osikowicz, W.; de Jong, M. P.; Salaneck, W. R. *Adv. Mater.* **2007**, *19*, 4213.

(94) Duhm, S.; Heimel, G.; Salzmann, I.; Glowatzki, H.; Johnson, R. L.; Vollmer, A.; Rabe, J. P.; Koch, N. *Nat. Mater.* **2008**, *7*, 326.

(95) Salzmann, I.; Duhm, S.; Heimel, G.; Oehzelt, M.; Kniprath, R.; Jonhson, R. L.; Rabe, J. P.; Koch, N. *J. Am. Chem. Soc.* **2008**, *130*, 12870.

(96) Chen, W.; Huang, H.; Chen, S.; Huang, Y. L.; Gao, X. Y.; Wee, A. T. S. *Chem. Mater.* **2008**, *20*, 7017.

(97) Duhm, S.; Salzmann, I.; Heimel, G.; Oehzelt, M.; Haase, A.; Johnson, R. L.; Rabe, J. P.; Koch, N. *Appl. Phys. Lett.* **2009**, *94*, 033304.

(98) Verlaak, S.; Heremans, P. *Phys. Rev. B* **2007**, *75*, 115127.

(99) Verlaak, S.; Rolin, C.; Heremans, P. *J. Phys. Chem. B* **2007**, *111*, 139.

(100) Morteani, A. C.; Dhoot, A. S.; Kim, J. S.; Silva, C.; Greenham, N. C.; Murphy, C.; Moons, E.; Cina, S.; Burroughes, J. H.; Friend, R. H. *Adv. Mater.* **2003**, *15*, 1708.

(101) Halls, J. J. M.; Walsh, C. A.; Greenham, N. C.; Marseglia, E. A.; Friend, R. H.; Moratti, S. C.; Holmes, A. B. *Nature* **1995**, *376*, 498.

(102) Arias, A. C.; MacKenzie, J. D.; Stevenson, R.; Halls, J. J. M.; Inbasekaran, M.; Woo, E. P.; Richards, D.; Friend, R. H. *Macromolecules* **2001**, *34*, 6005.

(103) Brabec, C. J.; Sariciftci, N. S.; Hummelen, J. C. *Adv. Funct. Mater.* **2001**, *11*, 15.

(104) Cao, Y.; Parker, I. D.; Yu, G.; Zhang, C.; Heeger, A. J. *Nature* **1999**, *397*, 414.

(105) Palilis, L. C.; Lidzey, D. G.; Redecker, M.; Bradley, D. D. C.; Inbasekaran, M.; Woo, E. P.; Wu, W. W. *Synth. Met.* **2001**, *121*, 1729.

(106) Kang, S. J.; Yi, Y.; Kim, C. Y.; Cho, C. W.; Noh, M.; Jeong, K.; Whang, C. N. *Synth. Met.* **2006**, *156*, 32.

(107) Kadashchuk, A.; Vakhnin, A.; Blonski, I.; Beljonne, D.; Shuai, Z.; Brédas, J. L.; Arkhipov, V. I.; Heremans, P.; Emelianova, E. V.; Bässler, H. *Phys. Rev. Lett.* **2004**, *93*, 066803.

(108) Rao, A.; Wilson, M. W. B.; Hodgkiss, J. M.; Albert-Seifried, S.; Bässler, H; Friend, R. H. *J. Am. Chem. Soc.* **2010**, *132*, 12698.

(109) Mulliken, R. S.; Person, W. B. *J. Am. Chem. Soc.* **1969**, *91*, 3409.

(110) Kanai, Y.; Grossman, J. C. *Nano Lett.* **2007**, *7*, 1967.

(111) Flores, F.; Ortega, J.; Vazquez, H., Phys. Chem. Chem. Phys. **2009**, *11*, 8658 and references therein.

(112) Bagus, P. S.; Staemmler, V.; Wöll, C. *Phys. Rev. Lett.* **2002**, *89*, 096104.

(113) Vázquez, H.; Gao, W.; Flores, F.; Kahn, A. *Phys. Rev. B* **2005**, *71*, 041306.

(114) Braun, S.; Salaneck, W. R.; Fahlman, M. *Adv. Mater.* **2009**, *21*, 1450.

(115) Lemaur, V.; Steel, M. C.; Beljonne, D.; Brédas, J. L.; Cornil., J. *J. Am. Chem. Soc.* **2005**, *127*, 6077.

(116) Brédas, J. L.; Calbert, J. P.; da Silva Filho, D. A.; Cornil, J. *Proc. Natl. Acad. of Sci. U.S.A.* **2002**, *99*, 5804.

(117) Crispin, X.; Geskin, V. M.; Crispin, A.; Cornil, J.; Lazzaroni, R.; Salaneck, W. R.; Brédas, J. L. *J. Am. Chem. Soc.* **2002**, *124*, 8131.

(118) Scholes, G. D.; Curutchet, C.; Mennucci, B.; Cammi, R.; Tomasi, J. *J. Phys. Chem. B* **2007**, *11*, 6978.

(119) Murdey, R. J.; Salaneck, W. R. *Jpn. J. Appl. Phys.* **2005**, *44*, 3751.

(120) Avilov, I.; Geskin, V.; Cornil., J. *Adv. Funct. Mater.* **2009**, *19*, 624.

(121) Cornil, D.; Olivier, Y.; Geskin, V.; Cornil, J. *Adv. Funct. Mater.* **2007**, *17*, 1143.

(122) Sushko, M. L.; Shluger, A. L. *Adv. Funct. Mater.* **2008**, *18*, 2228.

(123) Murdey, R. J.; Salaneck, W. R. *Jpn. J. Appl. Phys. Part A* **2005**, *44*, 3751.

(124) Osikowicz, W.; de Jong, M. P.; Salaneck, W. R. *Adv. Mater.* **2007**, *19*, 4213.

(125) Offermans, T.; van Hal, P. A.; Meskers, S. C. J.; Koetse, M. M.; Janssen, R. A. J. *Phys. Rev. B* **2005**, *72*, 045213.

(126) Marcus, R. A. *Rev. Mod. Phys.* **1993**, *65*, 599.

(127) Brédas, J. L.; Beljonne, D.; Coropceanu, V.; Cornil, J. *Chem. Rev.* **2004**, *104*, 4971.

(128) Clayton, A. H. A.; Scholes, G. D.; Ghiggino, K. P.; Paddon-Row, M. N. *J. Phys. Chem.* **1996**, *100*, 10912.

(129) Coropceanu, V.; Cornil, J.; da Silva Filho, D. A.; Olivier, Y.; Silbey, R.; Brédas, J. L. *Chem. Rev.* **2007**, *107*, 926–952.

(130) Newton, M. D. *Chem. Rev.* **1991**, *91*, 767. Senthilkumar, K.; Grozema, F. C.; Bickelhaupt, F. M.; Siebbeles, L. D. A. *J. Chem. Phys.* **2003**, *119*, 9809.

(131) Verhoeven, J. W. *Adv. Chem. Phys.* **1999**, *106*, 603.

(132) Troisi, A.; Orlandi, G. *J. Phys. Chem. A* **2006**, *110*, 4065.

(133) Yi, Y.; Coropceanu, V.; Brédas, J. L., J. Mater. Chem. **2010**, submitted.

(134) Burquel, A.; Lemaur, V.; Beljonne, D.; Lazzaroni, R.; Cornil., J. *J. Phys. Chem. A* **2006**, *110*, 3447.

(135) Norton, J. E.; Brédas, J. L. *J. Am. Chem. Soc.* **2008**, *130*, 12377.

(136) McMahon, D. P.; Troisi, A. *J. Phys. Chem. Lett.* **2010**, *1*, 941.

(137) Martinelli, N. ; Idé, J. ; Sanchez-Carrera, R. S. ; Coropceanu, V. ; Brédas, J.L. ; Ducasse, L. ; Castet, F. ; Cornil, J.; Beljonne, D. *J. Phys. Chem. C* **2010**, DOI: 10.1021/jp105843t.

(138) Pourtois, G.; Beljonne, D.; Cornil, J.; Ratner, M. A.; Brédas, J. L. *J. Am. Chem. Soc.* **2001**, *124*, 4436.

(139) Postcavage, W. J.; Sharma, A.; Kippelen, B. *Acc. Chem. Res.* **2009**, *42*, 1758.

(140) Aryanpour, K.; Psiachos, D.; Mazumdar, S. *Phys. Rev. B* **2010**, *81*, 085407.

(141) See, for example, Klessinger, M., Michl, J. *Excited States and Photo-chemistry of Organic Molecules*; VCH: New York, 1995.

(142) Jenekhe, S. A.; Osaheni, J. A. *Science* **1994**, *265*, 765.

(143) Wang, J. F.; Kawabe, Y.; Shaheen, S. E.; Morrell, M. M.; Jabbour, G. E.; Lee, P. A.; Anderson, J.; Armstrong, N. R.; Kippelen, B.; Mash, E. A.; Peyghambarian, N. *Adv. Mater.* **1998**, *10*, 230.

(144) Palilis, L. C.; Makinen, A. J.; Uchida, M.; Kafafi, Z. H. *Appl. Phys. Lett.* **2003**, *82*, 2209.

(145) Gebler, D. D.; Wang, Y. Z.; Blatchford, J. W.; Jessen, S. W.; Fu, D. K.; Swager, T. M.; MacDiarmid, A. G.; Epstein, A. J. *Appl. Phys. Lett.* **1997**, *70*, 1644.

(146) Ho, G. K.; Meng, H. F.; Lin, S. C.; Horng, S. F.; Hsu, C. S.; Chen, L. C.; Chang, S. M. *Appl. Phys. Lett.* **2004**, *85*, 4576.

(147) Giro, G.; Cocchi, M.; Kalinowski, J.; Di Marco, P.; Fattori, V. *Chem. Phys. Lett.* **2000**, *318*, 137.

(148) Granlund, T.; Pettersson, L. A. A.; Anderson, M. R.; Inganas, O. *J. Appl. Phys.* **1997**, *81*, 8097.

(149) Wang, Y. M.; Teng, F.; Xu, Z.; Hou, Y. B.; Wang, Y. S.; Xu, X. R. *Eur. Polym. J.* **2005**, *41*, 1020.

(150) Zhao, D. W.; Xu, Z.; Zhang, F. J.; Song, S. F.; Zhao, S. L.; Wang, Y.; Yuan, G. C.; Zhang, Y. F.; Xu, H. H. *Appl. Surf. Sci.* **2007**, *253*, 4025.

(151) Zhao, D. W.; Zhang, F. J.; Xu, C.; Sun, J. Y.; Song, S. F.; Xu, Z.; Sun, X. W. *Appl. Surf. Sci.* **2008**, *254*, 3548.

(152) Liao, J. L.; Chen, X. W.; Liu, C. Y.; Chen, S. A.; Su, C. H.; Sut, A. C. *J. Phys. Chem. B* **2007**, *111*, 10379.

(153) Yang, S. Y.; Zhang, X. L.; Hou, Y. B.; Deng, Z. B.; Xu, X. R. *J. Appl. Phys.* **2007**, *101*, 3.

(154) Yang, C. C.; Hsu, C. J.; Chou, P. T.; Cheng, H. C.; Su, Y. O.; Leung, M. K. *J. Phys. Chem. B* **2010**, *114*, 756.

(155) Huang, Y. S.; Westenhoff, S.; Avilov, I.; Sreearunothai, P.; Hodgkiss, J. M.; Deleener, C.; Friend, R. H.; Beljonne, D. *Nat. Mater.* **2008**, *7*, 483.

(156) Sreearunothai, P.; Morteani, A. C.; Avilov, I.; Cornil, J.; Beljonne, D.; Friend, R. H.; Philips, R. T.; Silva, C.; Herz, L. M. *Phys. Rev. Lett.* **2006**, *96*, 117403.

(157) Morteani, A. C.; Sreearunothai, P.; Herz, L. M.; Friend, R. H.; Silva, C. *Phys. Rev. Lett.* **2004**, *92*, 247402.

(158) Zhu, X. Y.; Yang, Q.; Muntwiler, M. *Acc. Chem. Res.* **2009**, *42*, 1779.

(159) Westenhoff, S.; Howard, I. A.; Hodgkiss, J. M.; Kirov, K. R.; Bronstein, H. A.; Williams, C. K.; Greenham, N. C.; Friend, R. H. *J. Am. Chem. Soc.* **2008**, *130*, 13653.

(160) Pereverzev, A.; Bittner, E. R. *J. Chem. Phys.* **2006**, *125*, 10496.

(161) Tamura, H.; Ramon, J.G. S.; Bittner, E. R.; Burghardt, I. *Phys. Rev. Lett.* **2008**, *100*, 107402.

(162) Tamura, H.; Bittner, E. R.; Burghardt, I. *J. Chem. Phys.* **2007**, *126*, 021103.